TÉCNICO LISBOA

3D printed organ models and patient-specific dosimetry for children with heart disease

Pedro António Freitas Silva

Thesis to obtain the Master of Science Degree in

Engineering Physics

Supervisor: Prof. Maria Teresa Ferreira Marques Pinheiro
Prof. Pedro Manuel Peixoto Teles

Examination Committee

Chairperson: Prof. João Pedro Saraiva Bizarro
Supervisor: Prof. Pedro Manuel Peixoto Teles
Members of the Committee: Prof. Matheus Savi
Prof. Horácio João Matos Fernandes

December 2020

Para os meus pais.

Acknowledgments

First and foremost, I would like to demonstrate my sincere gratitude to my supervisors Prof. Teresa Pinheiro and Prof. Pedro Teles for their guidance and support during the course of this thesis. A special acknowledgment has to be made to Prof. Matheus Savi, of the Instituto Federal de Santa Catarina in Brazil, who was always available to solve problems, explain or clarify procedures and was kind enough to print part of the models.

To Drª Marta António, Dr. Sérgio Laranjo, and to the director of the Centro de Referência de Cardiopatias Congénitas do Centro Hospitalar Universitário de Lisboa Central, Drª Fátima Pinto, for their interest and cooperation in this exciting interdisciplinary project. And to Diana Sanchez who, in challenging times and at the very last minute, stepped in and printed the remaining models.

For those who crossed my path at Técnico, I am not able to put in words my gratitude towards you. To everyone that took me on after I switched courses and whether by a small conversation, the long laboratory hours, the extensive study sessions or the unforgettable nights, you truly made these five years memorable and special.

To my lifelong friends, that have unconditionally supported me in every way imaginable through comforting words, shared laughter or a single glance not only in these five years but throughout my life. A thank you will never be enough.

Lastly, to my family: Mãe, Pai e Fi. Obrigado por todo o apoio incondicional e todo o carinho que me deram ao longo destes cinco anos. Apesar da distância física que nos separou a maioria do tempo, senti-vos sempre próximos de mim. Nada disto teria sido possível sem vocês e por isso estar-vos-ei sempre grato.

Resumo

O interesse e uso da impressão 3D para uso clínico tem crescido nos últimos anos, uma vez que esta tecnologia tem uma grande capacidade de produzir estruturas anatómicas com grande detalhe e replicar anomalias complexas.

O objetivo principal desta tese é criar modelos impressos em 3D do coração de crianças com cardiopatias, sejam elas congénitas ou adquiridas. Frequentemente, pacientes pediátricos com cardiopatias são submetidos a diferentes tipos de exames radiológicos ao longo da vida. A exposição precoce e prolongada é um motivo de preocupação uma vez que a exposição a radiação ionizante pode aumentar o risco de cancro ou outras doenças.

Os modelos foram produzidos a partir de dados de três pacientes, através de Tomografias Computadorizadas (TC) e Ressonâncias Magnéticas (RM), do Centro de Referência de Cardiopatias Congénitas do Hospital de Santa Marta, seguindo as normas nacionais de proteção de dados e padrões de ética.

Os modelos impressos apresentaram uma qualidade adequada de segmentação e impressão, reproduzindo com precisão as características anatómicas do coração e da vasculatura. No entanto, as limitações da TC em relação ao contraste para diferentes tecidos moles e a menor resolução da RM podem causar imperfeições localizadas nos modelos impressos em 3D.

Este tipo de tecnologia atualmente não está disponível no sistema de saúde português. Assim, ao oferecer à comunidade médica um método rápido para melhorar os resultados cirúrgicos e de intervenção, bem como os procedimentos de otimização da dose, tornar-se-á uma vantagem para os resultados finais e a qualidade de vida do paciente.

Palavras-chave: Impressão 3D, Cardiopatias, Radiação ionizante, Dosimetria.

Abstract

The interest and use of 3D printing in clinical applications has been steadily advancing in recent years given that this technology has a great capacity to produce increasingly detailed anatomical structures and replicate complex anomalies.

The main goal of this thesis is to create 3D printed models of the hearts of children with heart disease, whether congenital or acquired. Often, paediatric patients with heart disease are subject to different types of radiological examinations throughout their lives. This early and protracted exposure to ionising radiation is a source of concern as exposure may increase lifetime risk for cancer and other diseases.

The models were produced using data from three patients, through Computed Tomographies (CT) and Magnetic Resonances (MRI), at the Centro de Referência de Cardiopatias Congénitas do Hospital de Santa Marta, following national data protection norms and ethical standards.

The printed models showed an adequate quality of segmentation and impression, accurately reproducing the anatomical characteristics of the heart and vasculature. However, the limitations of CT in relation to contrast for different soft tissues and the lower resolution of MRI may cause imperfections located in 3D printed models.

This type of technology is currently not available in the Portuguese health care system. So, by delivering to the medical community a fast method to improve interventional and surgical outcomes, as well as dose optimisation procedures, it will become a clear advantage for the patient's outcome and quality of life.

Keywords: 3D printing, Heart disease, Ionising radiation, Dosimetry.

Contents

List of Figures

List of Abbreviations

ASD	atrial septal defect
CoA	coarctation of the aorta
CT	computed tomography
CHD	congenital heart disease
CAD	Computer-Aided Design
DICOM	Digital Imaging and Communications in Medicine
DLP	dose length product
ECG	electrocardiogram
FDM	fused deposition modelling
ICRP	International Commission on Radiological Protection
IR	ionising radiation
KD	Kawasaki disease
LAD	left anterior coronary
LAA	left atrial appendage
LCX	left circumflex artery
MRI	magnetic resonance image
RCA	right coronary artery
STL	Standard Tessellation Language
SLA	stereolithography
ToF	Tetralogy of Fallot
TLD	thermoluminescent dosimeter
3D	three-dimensional

TGA Transposition of the Great Arteries

2D two-dimensional

UV ultraviolet

VSD ventricular septal defect

Chapter 1

Introduction

1.1 Motivation

In the past years, the use of 3D printing in medicine has been increasing. This technology can create realistic, personalised and anatomically accurate models for niche applications specifically in Cardiology.

Heart disease, whether congenital or acquired, with diverse and sometimes complex pathologies would benefit from this technology by presenting a complete representation of the anatomy, bring out a deeper understanding of complex spatial relationships between different structures and providing a personalised treatment adequate to the patient [1].

Understanding and visualising the surgical anatomy from the images obtained through imaging methods is limited and requires a difficult process of mental reconstruction and can be often inadequate or incomplete [1, 2]. Furthermore, by using a patient-specific anatomical model of the heart, discussions within the medical teams managing complex cases will be facilitated, cardiologists may feel more prepared, and experienced surgeons and interventional radiologists can develop innovative approaches to cases, thus yielding better patient outcomes, lowering intervention time and re-intervention rate [3].

This type of technology can also serve as an educational tool to train students on more complex anatomy and allowing them to explore rare cases with detailed models. In addition, these models will be useful to patients and their families expanding their understanding of their condition and endow them with the necessary information in order to make informed decisions.

3D printed models may as well enable further developments in medical physics such as an accurate effective dose estimation; for instance, the tissue-weight dose quantity, in paediatric patients with heart disease that need diagnostic or interventional procedures that require radiation. Due to their condition, paediatric patients with congenital heart disease (CHD) are subject to various diagnostic X-ray examinations since the early stages of their lives. The optimisation of paediatric patient doses, still remains an unsolved question in diagnostic and interventional radiology [4]. Therefore, to solve this issue, a wide range of dosimetric measurements has to be made from all ages, extending from a neonate to an adult, to ensure that the findings are the most accurate possible.

The aim of this thesis is to create 3D printed models of the hearts of children with heart disease.

Moreover, these models can be used to estimate the dose received in the CT procedure and eventually contribute to an optimisation of protocols for children from newborn to older ages.

This thesis offers the opportunity to work in a multidisciplinary environment, with physicists, physicians, radiologists among others. It is in the scope of a collaborative project with the group of Professor Matheus Savi of the Instituto Federal de Santa Catarina, Brazil.

1.2 Heart disease in paediatric ages

Heart disease is an umbrella term to describe a range of conditions that affect the heart. Among these conditions are heart defects that are present since birth, congenital heart disease; and conditions that develop during a person's lifetime, acquired heart disease.

CHD is a structural or functional defect of the cardiovascular system that is present since birth. The prevalence of CHD is 8 cases per 1000 births and are considered the most common congenital malformation [5, 6].

Some of the more common defects include Tetralogy of Fallot (ToF); Coarctation of the aorta (CoA) and Transposition of the Great Arteries (TGA) [6]:

- **ToF** represents about 10% of congenital heart defects. It consists on four structural defects: ventricular septal defect, pulmonary valve stenosis, overriding aorta and right ventricular hypertrophy [6, 7]. It has a similar incidence between males and females. The definite treatment is surgical and can be performed in childhood [5, 6]. The prognosis is dependent on repair of outgoing corrective surgery tract.

- **CoA** has an incidence of 3 to 4 in 10000 live-births, constitutes about 5 to 7% of CHD patients and is more common in males. Often, it presents itself in the neonatal period and early childhood [7, 8]. It consists of a constrictions in a portion of the aorta, which forces the heart to pump harder to get blood through the aorta and on to the rest of the body. These patients maintain, in the long run, significative morbidity and mortality rates compared to the general population.

- **TGA** accounts for 5% to 7% of congenital heart defects and it is the most diagnosed congenital heart defect during the neonatal period. TGA can be described by a transposition of the aorta and the pulmonary artery, meaning that opposite to a normal heart, the aorta rises from the right ventricle and the pulmonary artery arises from the left ventricle. This causes the oxygen-poor blood from the body to enter the right side of the heart through the aorta being pumped directly back out to the rest of the body through the aorta, and the oxygen-rich blood from the lungs enters the left side of the heart being pumped back to the lungs through the main pulmonary artery. [5, 7]. It has an incidence of 2 to 3 cases in 10000 live-births having predominance in males (60-70%). When not treated, TGA presents a mortality of 29% in the first week of life and 89% in the first year depending on the presence of other heart defects. The definite treatment is surgical. The survival rate is more than 90% in 15 years, with no need of reintervention in 80 to 85% of cases [7].

Acquired heart disease is a condition that affects the heart and the surrounding blood vessels that develops during a person's lifetime at any age, unlike CHD that is present since birth.

- **Kawasaki disease (KD)** is the leading cause of acquired heart disease in developing countries [5, 6, 9]. It is a child vasculitis that is characterised by the inflammation of small to medium arteries that can lead to the formation of coronary aneurysms [5, 6]. Its incidence varies according to location, being more common in children of Asian descent; in Portugal, the incidence is about 6.5 per 100000 children younger than 5 years of age [9]. It has a predominance in males and commonly occurs in children younger than 5 years of age [6].

In order to improve the outcomes of patients with CHD, an early and precise diagnosis is necessary to decide handling strategies and treatment [10]. Cardiac imaging is a key element in paediatric cardiology being indispensable at all stages of patient care [11].

1.3 Clinical imaging methods in paediatric cardiology

Imaging provides a comprehensive and complete anatomical description of the structures and physiology of CHD [11]. Due to current advancements in CT and MRI imaging techniques these modalities have become convenient supplements in the imaging of heart defects. Moreover, these techniques have a paramount role through being able to provide a preferable anatomical representation and aiding in pre-operative planning and post-operative management [10].

1.3.1 Computed Tomography

A computed tomography (CT) is a computerised imaging procedure that, by scanning the area of interest with a rotating X-ray beam, produces images of each cross section by combining the measurements from different angles [12].

The CT process can be described by three components: data acquisition, image reconstruction, and image display.

In order to acquire the information, the rotating X-ray tube (figure 1.1) produces a beam of X-ray photons for each rotation that irradiates a section of the patient's body. These photons can either be fully absorbed or they can be attenuated then being able to strike the detectors [12, 13].

The photons that reach the detectors are converted to an electrical signal being later compiled with the data from the other detectors into a matrix. The system assigns each pixel in the matrix a number that represents the tissue attenuation, in Hounsfield units, that represent the average of all attenuations for that pixel [12, 13].

Eventually, this data is processed using tomographic reconstruction that produces a series of cross-sectional images. The resulting CT images are displayed by varying shades of gray in terms of radiodensity [12, 13].

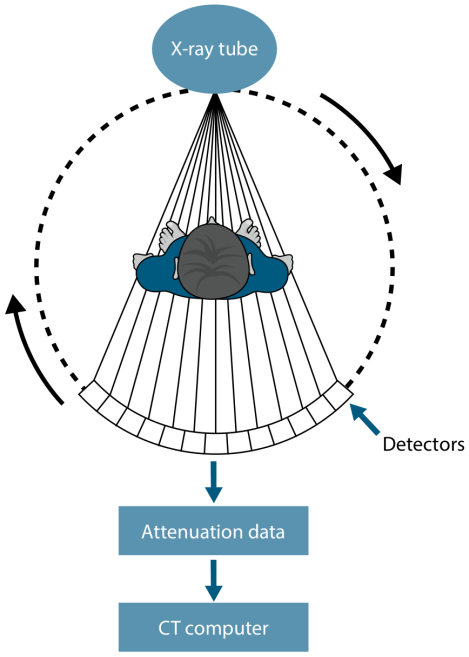

Figure 1.1: Schematic illustration of the CT system. Retrieved from [13].

In contrast to a conventional radiography, the CT scan greatly diminishes the superimposition of structures outside the area of interest, has faster scan times, a greater spatial resolution, an excellent differentiation between different types of tissues and, in cardiology, the heart and adjacent structures are more defined when using a CT as an imaging method [7, 12, 14]. CT scans can be performed in patients that have metallic or electronic implants and pacemakers [14].

Motion of any kind creates artifacts and parts of the image can become blurry causing degradation of the image. Thus, performing a CT scan in children is often challenging as it may be difficult for them to hold their breath and to stay immobilised during an adequate period of time. This can lead the formation of motion artifacts in the final image. Fast scan speeds cannot compensate for sudden movements [7].

Since typical scan takes seconds to perform, in order to bypass this issue anaesthesiologists have access to short-acting sedative drugs to avoid movement from the patient. Breath-holding can be achieved using the controlled ventilation technique with a face mask as the open environment around the CT scanner permits access to the face of the patient [7, 15].

The CT imaging quality is also dependent on the level of aortic enhancement caused by the bolus of iodinated contrast media that is administrated intravenously. The contrast bolus requires adequate delivery and timing. With the purpose of limiting the radiation exposure as low as reasonable achievable, the imaging has to be synchronised with the peak of enhancement in the region of interest caused by the delivery of the contrast bolus [7]. Other measures can be taken to reduce dose without compromising the image quality such as having as low as possible settings of power (kV) and current (mA) of the X-ray tube [14].

The International Commission on Radiological Protection (ICRP) has estimated that a CT chest for children younger than 5 years of age has an effective dose around 1.5 mSv (ICRP 60 [16]) and 1.8 mSv (ICRP 103 [17]). These values were calculated using mean dose length product (DLP) values combined

with age-specific and region-specific conversion factors [16–18].

Even though there is a lack of knowledge on low-dose radiation exposure in paediatric ages, ionising radiation (IR) is a known carcinogen to which children are particularly vulnerable since the radiosensivity is highest in early life therefore the associated risk to irradiation in childhood is significantly higher than in adulthood [4, 14, 19]. Due to their condition, paediatric patients with congenital heart disease are subjected to various IR diagnostic examinations since the early stages of their lives.

Granted that the mechanisms conveying greater vulnerability to radiation exposure in children are still not clarified, repeated exposure to IR and accumulated DNA damage will possibly set the stage for the development of radio-induced pathologies later in life [20]. This increased risk could greatly affect the lives of these children, their families and carers.

The European Commission guidelines on radiation protection [4], initiatives congregating health care institutions worldwide, for instance Image Gently “Have-A-Heart” campaign [21], as well as American and European paediatric cardiology associations have identified the paediatric patient dose optimisation as a major quest in diagnostic and interventional radiology. Reason is that prolonged exposure to IR procedures in early ages may increase risk of developing diseases later in life. Risk prediction is a function of survival and attained age but it is also a function of cumulative dose and organ exposure. Convincing scientific evidence has recently made available, which demonstrated that adults with CHD had a 1.6–2 times higher prevalence of cancer than the general population [19].

Even if the benefit of diagnosis and treatment using IR-based procedures in children with CHD is immense and frequently lifesaving, there is a need to implement methodologies encompassing biological, physical and technological approaches, to quickly report effective and organ doses and to minimize exposure to IR in early life without sacrificing the quality of care. These measures will be very important to reduce long-term negative health effects [22–24].

1.3.2 Magnetic Resonance Imaging

A magnetic resonance image (MRI) is a non-invasive imaging technology that uses nuclear magnetic resonance to generate images. It depends on the interaction between an external magnetic field and the spin of the nucleus of interest [25]. Even though certain nuclei possess a nuclear magnetic moment, only the hydrogen nuclei found in water, fat and other tissues such as the cardiac tissue and vessels, can provide a sufficient signal to create an image of the scanned region in terms of the density of those nuclei [26].

By applying an external magnetic field, the nuclei become polarised producing a net magnetisation aligned with the field. Furthermore, by applying a pulse of energy at the Larmor frequency using the RF coils (figure 1.2) the hydrogen protons are excited. The energy is absorbed and then re-emitted that is measured as the signal by a receiving coil [25].

In order to encode position information an additional magnetic field is applied using the gradient coils (figure 1.2). This additional magnetic field causes the nuclei to resonate at different frequencies depending on their location thus being able to retrieve information about the spatial locations [25].

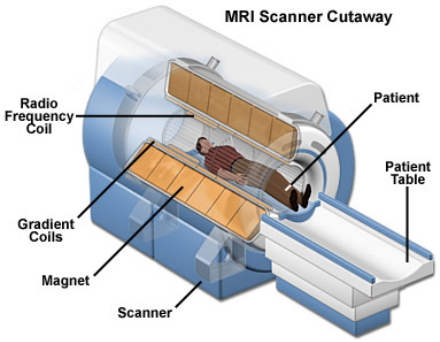

Figure 1.2: Schematic illustration of the MRI system where the main components are indicated. Retrieved from [27].

Compensation for respiratory motion is vital in a MRI scan and can often be challenging in children. The most common approach to compensate for this motion is to gate the image acquisition with the cardiac cycle. The cardiac cycle can be tracked using the electrocardiogram (ECG). Seemingly, a high-quality ECG signal is essential to guarantee a good image quality [7, 28].

Although motion artifacts caused by cardiac motion can be compensated by an ECG-gated MRI, a MRI scan can take up to 60 minutes and motion artifact has to be minimised during image acquisition as previously mentioned [7]. A common practice to overcome this issue is to sedate or anaesthetise most patients younger than 6 years of age. Before the MRI scan, a careful preparation involving the risks and benefits of undergoing the examination under sedation or anaesthesia should be well determined since it has a beneficial effect [7, 14]. However, this practice can vary given that multiple factors are taken into account when pondering a sedated examination like the length of the protocol examination, the maturity of the child, experience with prior procedures and anaesthetic support [7, 14]. General anaesthesia is the preferred sedation method over sedation with medication considering it is safe, achieves adequate sedation, offers control of ventilation and protects the airway [7].

1.4 Thesis outline

The first two chapters of this thesis explain the important concepts concerning heart disease, imaging procedures and 3D printing. Furthermore, they show the importance of developing new technological tools such as 3D printed models and how do these models improve treatment of children with heart disease. Chapter 1 provides an overview on heart disease and imaging methods focusing on the challenges these procedures face while being performed in paediatric patients and methods to improve the image quality. Chapter 2 presents a review of 3D printing including the printing techniques, the applications in medicine and the limitations of these models. Chapter 3 provides the fundamental notions about the anatomy of the heart to be used in the segmentation process and presents the methods that are going to be used in the segmentation and printing processes. Chapter 4 presents the cases subject to study, the segmentation and printing processes and, the feedback from the doctors. Finally, Chapter 5 lays out the final conclusions, whether or not the proposed objectives were met, what was achieved with the work of this thesis and future prospects.

Chapter 2

3D printing

Three-dimensional (3D) printing is a technique that is used to transform digital models into physical models. The technology was first introduced in 1986 and since then it has grown to encompass different manufacturing technologies for various applications in different areas. From the beginning of this millennium - when the first paper regarding cardiac application of 3D printing was published - to now, 3D printing has been used in the diagnosis, management and education in heart disease [2, 29].

The process of 3D printing applied to medicine can be summarised by the acquisition of a imaging data-set through an imaging procedure (figure 2.1a and 2.1b); the segmentation of the anatomy using specialised software (figure 2.1c); design refinement such as the addition of cut-planes and model stability elements using Computer-Aided Design (CAD) software; the Standard Tessellation Language (STL) file conversion (figure 2.1c) and finally printing the physical model (figure 2.1d) [30].

(a) Imaging procedure. (b) Imaging dataset. (c) Segmentation and conversion to a STL file. (d) Model printing.

Figure 2.1: 3D printing process. Retrieved from [3].

The segmentation process allows for the separation of the different structures from the imaging datasets using a reconstructed model derived from the two-dimensional slices from the imaging datasets. Using contrast agents on imaging procedures allows the distinction of the cardiac and blood pool volumes. The following process is semi-automated using software algorithms: boundaries detection and signal threshold where pixels with the same intensity are grouped. Although these algorithms are crucial to ensure quality segmented images, visual editing is always necessary to guarantee that all structures have been accurately delineated and that the final result is a precise representation of the target anatomy [29, 31].

After segmentation, the Digital Imaging and Communications in Medicine (DICOM) image files have

to be converted into the STL format since 3D printers don't recognise DICOM files. The STL format defines surfaces as small triangles that fit together. Often, the conversion process produces defects in the model consequence of artifacts present in the image files. These defects have to be eliminated since 3D printers can only utilise complete STL files. STL models can be modified with CAD software to achieve a certain purpose such as making a certain pathology visible or removing structures that are not of interest [29, 31].

2.1 Printing techniques

A variety of printing techniques are available and meet the needs in cardiovascular medicine and surgery:

- *Stereolithography* is an additive manufacturing process that uses a technique based on a layer-by-layer photopolymerisation, that is, a digitally guided ultraviolet (UV) laser light is used to harden the surface layer of the polymer liquid [29, 31];
- *Fused deposition modeling* technology deposits a continuous filament of melted thermoplastic layer-by-layer as the material hardens after the extrusion [29, 31];
- *PolyJet technology* creates 3D models by jetting thin layers of liquid photopolymers that are hardened by using UV light. This technology can incorporate multiple materials and colours simultaneously acting as an advantage against other techniques because it has the capability of highlighting certain pathologies or implants and it being visible from the surrounding native printed tissue [29, 31];
- *Selective laser melting* creates strong model parts using fused metal or ceramic powder using a high-power laser. It is preferred for building functional prototypes such as native valves or medical implants. Its use is still limited due to the high production costs [29, 31].

2.2 Applications

2.2.1 Teaching tools

3D printed models applied to education and training is already an established practice in neurosurgery, otolaryngology and more recently cardiology. While the practice of *"see one, do one and teach one"* has been the standard in medical training, the utilisation of 3D models in physician education represents a change from the apprenticeship model to learning based on simulation that complements the traditional mentored training [30].

The learning curve for cardiac trainees can be reduced with the use of 3D models by understanding more easily the complex anatomies present in heart defects, having high-fidelity simulation experiences and being exposed to rare cases. The supervisor can take unlimited time in showing procedures and

trainees can take enough time to practice and repeat the procedures until they feel confident. All these key areas shift the surgery practice from an *opportunity-based* experience to a *curriculum-based* experience. These models can further be used for lifelong learning, maintenance of certification, practice before challenging cases or even, for experienced surgeons, to develop new procedures [2, 30].

2.2.2 Procedural planning

Heart diseases are often connected with complex and unique anatomies, thus being hard to fully evaluate the defects from two-dimensional (2D) CT or MRI images. 3D printed models can play an important role in comprehension and assessment of functionality of various heart conditions [29]. Additionally, as thoraxes and heart sizes are small in children, the surgical scene is difficult to assess from the assistant's position during the surgical procedure. Therefore, sterilised models would pose as an advantage since pre-operative planning and simulation may be made; the surgical procedure can be facilitated by easily providing structural anatomic orientation and precise cooperation from the assistants; and for further testing novel procedural pathways [2, 29].

In regards to surgical simulation, the current print materials are still far from ideal considering that they do not represent the cardiac tissue properties hence limiting the assessment of tissue response. Nonetheless, surgeons find the models suitable for practicing surgical procedures [2].

2.2.3 Device Innovation

The capability of testing structural heart repair devices on a set of cardiac pathologies is appealing. Despite modeling options such as device modeling using cadaveric models or even using animal models have been relied for many years it cannot be used for patient-specific procedure planning. Hence, the creation of an accurate patient-specific 3D model has all of the characteristics of a detailed digital model and also provides an accurate evaluation of the consequences of the anatomical relations that are influenced by the implanted devices [29].

2.2.4 Dosimetry

According to an European report, the number of interventional cardiology procedures in Portugal is increasing at a typical rate of 6.8% [32]. Although imaging procedures that utilise ionising radiation always have advantages in diagnosis and treatment, the radiation-dose levels in these procedures have been raising some concerns; these concerns are heightened in paediatric cardiology since children have higher radiosensitivity than adults [4, 32].

Current effective dose estimation methodologies rely on the calculation of the DLP and a conversion factor based on the region of the body that underwent through the ionising radiation procedure established by Monte Carlo simulations. Considering these estimation methodologies have varying degrees of effective dose agreement, the estimates for the same type of procedures on different patients may differ because of the methodology used [4, 21].

By reproducing the volume, cavities and major vasculature, the 3D printed model of the heart can be used to determine the effective dose received on an ionising radiation procedure by mimicking the children's thorax with a phantom where the model is inserted and dosimeters are placed on the surface and inside the organ model so acquisitions can be made. This type of technology can be used to create a patient radiological record, a necessary tool to assess the lifetime risk for cancer and other diseases due to the dose received through imaging procedures since patients with heart disease are more likely to develop radiation exposure related cancer from cardiac imaging [19].

The model may be printed with a material that successfully resembles the cardiac tissue physical properties; that way, the cardiac tissue radiation attenuation is precise and the dosimeter readings are as accurate as possible.

2.3 Limitations of 3D printed models

The limitations of 3D printing occur in all stages of the process since imaging, post-processing and printing. With the current imaging procedures, it is strenuous to image with accuracy and precision fine moving anatomical structures. This poses as a problem since abnormalities in these structures are associated with functional consequences and require delicate surgical repair [2].

As previously mentioned, the segmentation process is facilitated by software algorithms that rely on thresholding signal intensities. Extensive manual editing is necessary when the adjacent structures do not differ that much on signal intensities. The accuracy of the model is naturally compromised considering that the final result is operator dependent: bias could be introduced in all steps from image acquisition to the choice of areas to be segmented [1, 2].

When the main goal is visualisation of the anatomic relationship of specific structures, a simple printed model can be constructed using a single rigid material. However, when practice procedures are to be performed in the model itself, it is ideal to print said model with more flexible materials that can accurately replicate cardiac tissue mechanics with similar physical properties. Flexible materials that are currently available are not satisfactory for surgical practice; surgeons find the models made of these materials to be more difficult to handle than real cardiac tissue [1, 2, 29]. Additionally, an accurate comparison between cardiac tissue and printing materials can be questionable since there is variation in tissue properties with aging; mechanical differences of cardiac structures during the static and functional states; and scarce amount of data with respect to the cardiac mechanical properties meant for 3D print replication [29].

Chapter 3

Methodology

3.1 Anatomical structures of the heart

3.1.1 Terminology

In order to provide a comprehensive explanation of the structures and their relative position in the body, some terminology has to be presented particularly directional terms and the body planes.

The directional terms are based on the body being viewed in the anatomic position i.e. from the point of view of the subject, not the observer [12]. The term anterior refers to movement or structure towards the front of the body while posterior regards to movement or structures towards the back of the body. Inferior describes downward movement or describes a position below another part of the body. On the contrary, superior defines upward movement or to classify a position above another part of the body [12].

A body plane represents a section of the body, where a section is a two-dimensional surface of a cut three-dimensional volume (figure 3.1) [33]. Axial planes are horizontal cross-sectional planes that divide the body into a superior and an inferior section. The sagittal plane splits the body into the left and right sections. Lastly, the coronal plane separates the body into anterior and posterior sections. Oblique planes are sections that lie at an angle to one of the three standard planes [12].

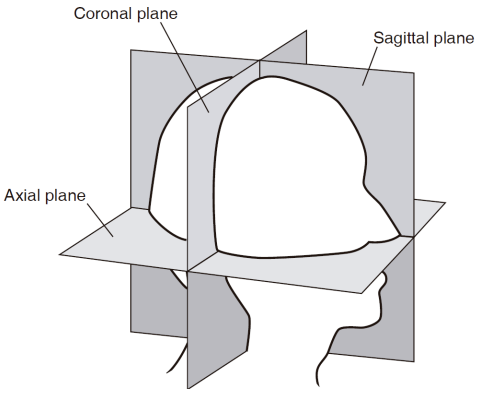

Figure 3.1: Imaging planes. Retrieved from [12].

3.1.2 Substructures of the heart

The heart is a hollow muscular organ that lies in the midline of the thoracic cavity and plays a central role in the cardiovascular system [34]. It is divided into two halves, referred as left heart and right heart, and each half is divided into two chambers, the upper being named atrium and the lower the ventricle. The ventricles are separated from each other by the interventricular septum (figure 3.2).

In addition, the heart has four valves that separate its chambers and allows blood flow in only one direction in the heart. The valves between the atria and ventricles are called atrioventricular valves: the valve that lies between the right atrium and right ventricle is called the tricuspid valve; and, between the left atrium and left ventricle is the mitral valve (figure 3.2) [35]. Two other valves sit at the exit of each ventricle. The pulmonary valve is located between the right ventricle and the pulmonary trunk, and the aortic valve is based among the left ventricle and aorta (figure 3.2) [35].

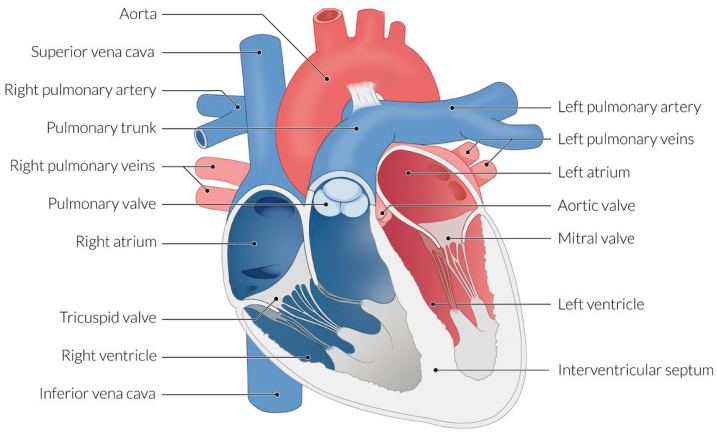

Figure 3.2: Illustration of the frontal section of the human heart. Retrieved and adapted from [36].

The right atrium receives the low-oxygen blood (venous blood) from the superior and inferior venae cavae, it is pumped to the right ventricle further delivering the blood to the pulmonary circulation where it is oxygenated. The oxygenated blood (arterial blood) flows into the left atrium, passing to the left ventricle that pumps it to the rest of the body [34, 37, 38].

The great vessels bring blood to and from the heart. They include the aorta that distributes the oxygenated blood to the body and commences at the upper part of the left ventricle; the pulmonary artery that carries deoxygenated blood to the lungs and begins at the base of the right ventricle; and the superior and inferior venae cavae that deliver blood from the body into the right atrium (figure 3.3).

Additionally, the coronary arteries supply oxygenated blood to the cardiac tissue. They arise from the ascending aorta and supply oxygenated blood to the muscle and other tissues of the heart. Its two main branches are the right coronary artery (RCA) and the left coronary artery that bifurcates into the left circumflex artery (LCX) and the left anterior coronary (LAD) [39].

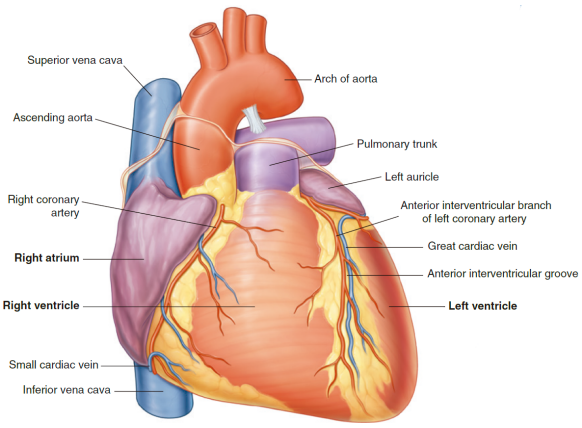

(a) Anterior view of the heart.

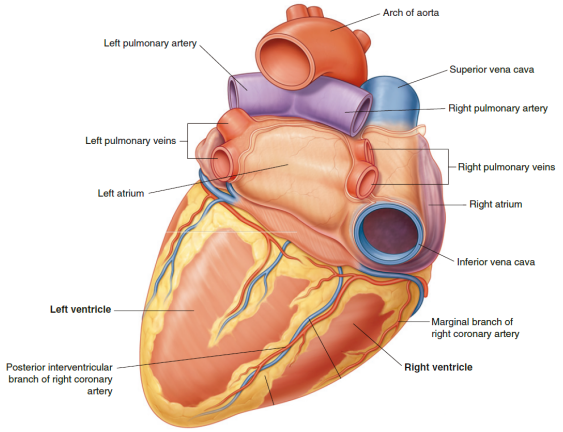

(b) Posterior view of the heart.

Figure 3.3: Diagrams showing the different components of the heart anatomy. Retrieved and adapted from [39].

3.2 Imaging techniques

The CT data was obtained from a state-of-the-art 128-slice CT scanner SOMATOM Definition Flash (Siemans, Erlangen, Germany) using an iodinated contrast medium at Hospital de Santa Marta, Lisbon. All the data covered the whole heart from the upper abdomen to the aortic arch. The average axial slice thickness is 0.40 mm and the resulting images have a resolution of 512×512 pixels.

The MRI data was acquired by the MRI scanner Optima™ MR450w (GE Healthcare, Chicago, United States of America) being administered a gadolinium contrast medium at Hospital de Santa Marta in Lisbon. The scans covered the whole heart from the upper abdomen to the aortic arch. The average axial slice thickness ranges from 1 mm to 1.2 mm and the resulting images have a resolution of 512×512 pixels.

3.3 Segmentation methodology

As mentioned in section 2, segmentation is a process that allows for the separation of different regions or to delineate boundaries of these regions. The main goal of whole heart segmentation is to extract and separate the desired information like the volume and shapes of the substructures of the heart [40, 41].

Considering we are working with paediatric patients with heart disease, a vast array of dispositions of structures in different subjects exists therefore a fully automatic segmentation is not possible. A semi-automatic method with an image-driven segmentation technique is preferable [38].

The thresholding method may be used to localise and extract a region of interest based on the analysis of the intensity histogram. This histogram is built as a discrete distribution of pixel intensities, by comparing the counts and values. Pixels that belong in the same intensity interval may belong to the same tissue. This method is effective when there is a clear distinction of intensity between the

area of interest and the surrounding areas. Occasionally, the intensity of different tissues overlap and the thresholding also encompasses other structures. In these cases, manual editing is necessary to eliminate the selection of non-desired structures in the segmentation [1, 2, 38, 41].

Hence, manual labelling accompanied with the thresholding method was adopted to generate the segmentation. The segmentation was performed by using the open-source software 3DSlicer [42]. The axial, sagittal and coronal view (and sometimes transversal views) were visualised simultaneously in order to easily identify the structures, and to check the consistency, smoothness and to overall aid the segmentation process [43]. After the segmentation is finished and ready to be printed the software converts and exports the segments into the STL format.

3.4 Printing methodology

In this thesis, two types of printing techniques were used: fused deposition modelling and stereolithography. These techniques were briefly described in section 2.1.

Fused deposition modelling (FDM) is one of the most used 3D printing process due to its high-reliability, low costs and simplicity. The technique is based on the extrusion and then deposition of molten thermoplastic filament onto a platform, fabricating parts layer-by-layer (figure 3.4) [44]. Most of the segments were printed using this technology with the Pro Core H4 (GTMax3D, São Paulo, Brazil), Ultimaker 3 and Ultimaker 2 Extended+ (Ultimaker, Utrecht, The Netherlands) in combination with ABS filaments (3D.on, Florianópolis, Brazil) and PLA filaments (Alcia 3DP, Spain).

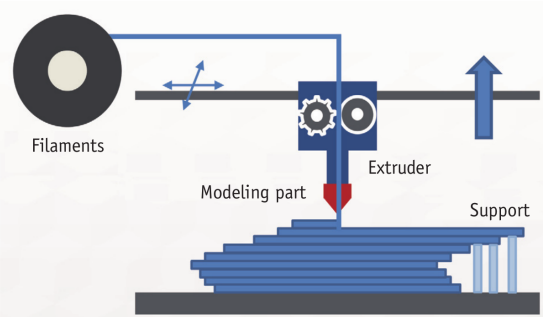

Figure 3.4: Illustration of the FDM technique. Retrieved from [45].

Stereolithography (SLA) was the first additive manufacturing process to be developed in the 1980s and has withstood the test of time on account of its accuracy, high precision, ability for fine details and its celerity. This procedure works in the layer-by-layer fashion using a guided UV light that leads to the solidification of a liquid resin by photopolymerisation (figure 3.5) [46]. On the segments that presented intricate and fine details this technique was chosen to manufacture more robust outcomes. The models were printed with the Photon S (Anycubic, Shenzhen, China) using a 405 nm Resin (Anycubic, Shenzhen, China).

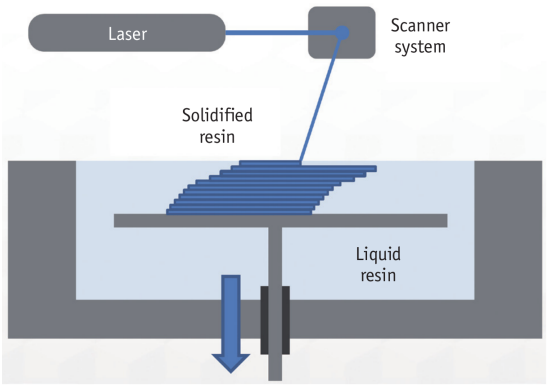

Figure 3.5: Illustration of the SLA technique. Retrieved from [45].

Following the conclusion of the segmentation and having the model in the adequate format, all files have to be imported into a slicing software. This kind of software automatically converts the STL format into specific printing commands usually expressed in G-code. The used slicing softwares were Simplify3D (Cincinatti, United States of America) and Cura (Ultimaker, Utrecht, the Netherlands).

Additionally, as a means to ensure that the printed model has good quality, the slicing software has supplementary features such as: infill that characterises the amount of material printed allowing the volume to be converted into a hollow one with partially filled internal structures that might save material and time; supports that are easily detachable for parts that do not have any layers below and need a foundation to maintain structural stability; and the base layer that consists in the printing of the first layer that is easily detachable in order to overcome issues of lack of adherence to the printing bed, rugosity and to secure smooth deposition of the filament.

3.5 Case studies

The imaging data used in this study has been anonymised following the national regulations of data protection (Regulamento Geral de Proteção de Dados, 2018). The clinical protocols in force at the Centro de Referência de Cardiopatias Congénitas (CRCC), Hospital de Santa Marta, Centro Hospitalar Universitário de Lisboa Central (CHULC), together with informed consent, data registry and anonymity requirements at hospital level have been validated by the Ethical Committee Board of CHULC.

3.5.1 Case 1 - Kawasaki Disease

The first case is of a paediatric patient with Kawasaki disease (KD). As it was mentioned on section 1.2, KD is characterised by an inflammation of small to medium arteries that can lead to the formation of coronary aneurysms therefore the coronary arteries are the focal point.

It was decided that the adequate imaging procedure would be a CT due to the great spatial resolution and the greater structure definition ensuring then a superior image quality. In order to assure that the radiation exposure was as low as reasonably achievable, it was administered an iodinated contrast

bolus and the imaging was performed at the peak of enhancement in the region of contrast, this case the coronary arteries; this was also combined with low settings of the tube current and kilovoltage.

The CT scan revealed enlarged coronary arteries as expected (figure 3.6).

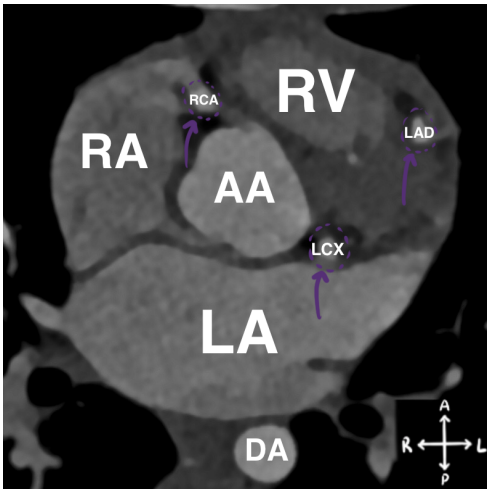

Figure 3.6: CT scan of the heart of a KD patient. The enlarged coronary arteries are clearly seen (purple circles and arrows). Axial view at the level of the left ventricle outflow.

3.5.2 Case 2 - Tetralogy of Fallot

The second case is of a paediatric patient with a surgically corrected Tetralogy of Fallot (ToF). ToF is usually characterised by four defects: pulmomary valve stenosis (narrowed exit of the right ventricle); ventricular septal defect (hole between the two ventricles); overriding aorta (blood from both ventricles) and right ventricular hypertrophy (thickening of the right ventricle muscle).

Both CT and MRI were performed in this case to combine the CT's significant spatial resolution and structure definition and the MRI's excellent soft tissue distinction and the ability to perform functional studies. With the interest of ensuring the best image quality possible and as low as reasonably achievable radiation exposure, an iodinated contrast bolus and a gadolinium contrast medium were administered in the CT and MRI, respectively.

The CT and MRI scan portrayed a discrepancy on the size of the left and right branch of the pulmonary artery; the right branch is small and short while the left branch has a substantial size (figure 3.7).

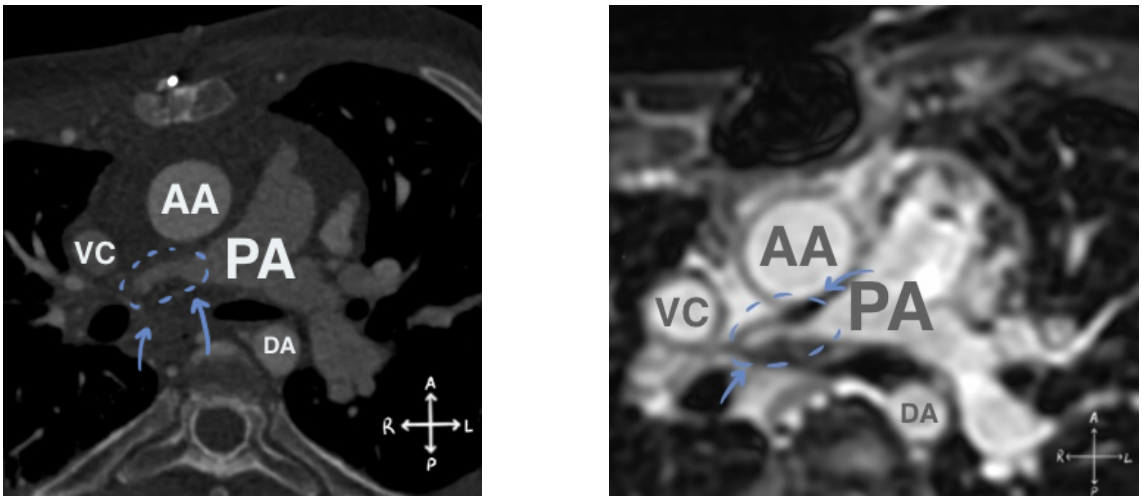

(a) CT scan. (b) MRI scan.

Figure 3.7: Disparity in sizes of the left and right branches of the pulmonary artery. The right branch is very small in contrast with the left branch (blue circles and arrows). Axial view.

In addition, both scans illustrated the surgically corrected pulmonary valve stenosis with presence of grooves on the exit chamber of the right ventricle (figure 3.7).

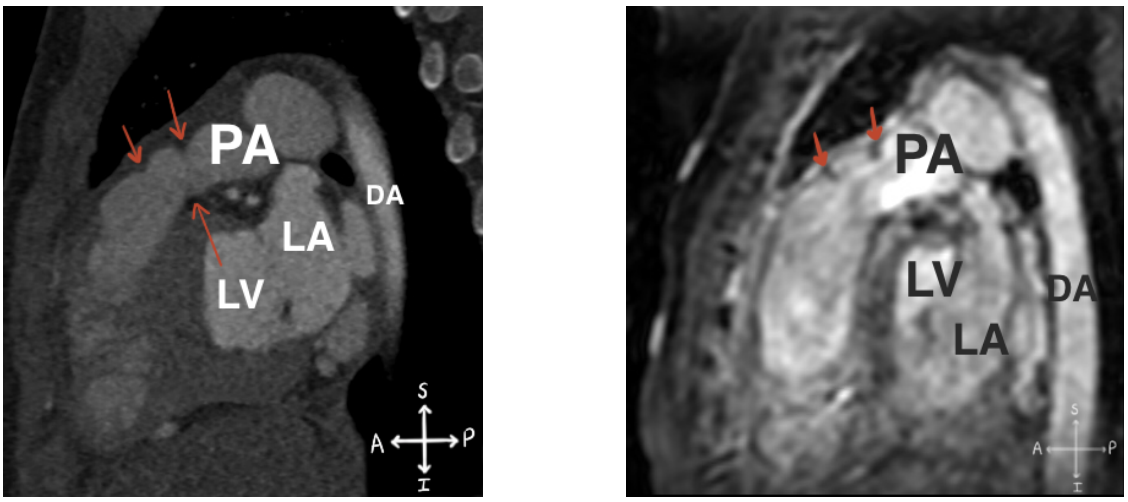

(a) CT scan. (b) MRI scan.

Figure 3.8: The grooves on the exit chamber of the right ventricle (red arrows). Saggital view.

3.5.3 Case 3 - Complex congenital heart disease

The third case is of a paediatric patient with a surgically corrected complex CHD. This case is characterised by a dextrocardia - where the apex of the heart is located on the right side of the body [47] -, only one atrioventricular valve and, it also has two superior venae cavae (one left and one right) each connected to their respective ipsilateral pulmonary arteries. Only a MRI scan was performed due to the need to perform a functional study on the patient to assess the tissue behaviour post-surgery. Again, the MRI scan was carried out using a gadolinium contrast medium to secure a good distinction between different structures.

The MRI scan showed the presence of two superior venae cavae (SVC), one on the right and one on the left. This becomes visible on the axial and the coronal view (figure 3.9).

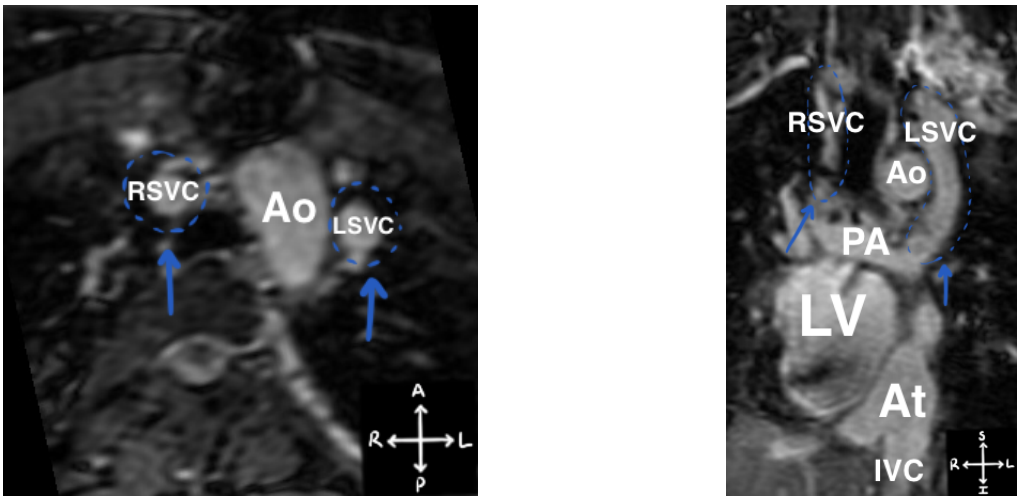

(a) Axial view.

(b) Coronal view.

Figure 3.9: MRI scan of a heart of a patient with complex CHD. It shows the presence of two venae cavae (blue circles and arrows).

Additionally, it corroborates the dextrocardia since the apex points towards the right not the left as usual. Furthermore, it also depicted the only atrioventricular valve present in the heart (figure 3.10).

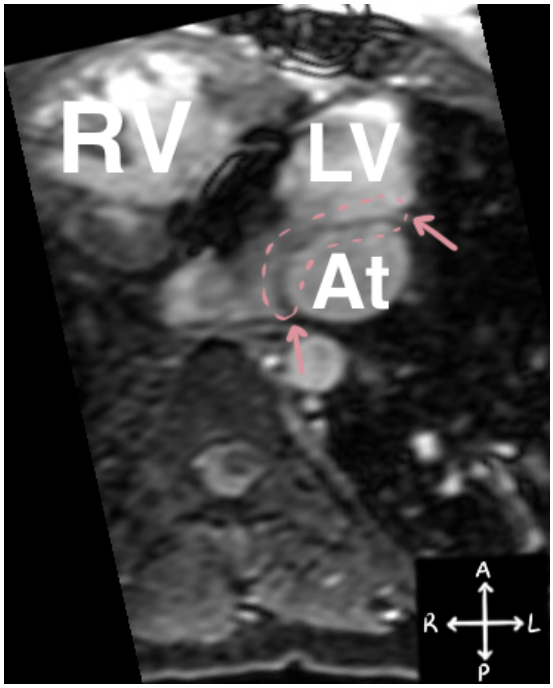

Figure 3.10: MRI scan of a heart of a patient with complex CHD. It that shows the present dextrocardia (the apex points towards the right) and the only atrioventricular valve (pink circle and arrows). Axial view.

Chapter 4

Results

4.1 Case 1 - Kawasaki Disease

The CT scan of the heart of the patient with KD had an overall good quality, with a clear distinction between different types of tissues, and properly displayed the coronary arteries which were the focal point of this scan. However, there is an artifact on three consecutive axial slices where different parts are superimposed, causing a slightly confusing set of frames that could originate a marginally different end result than expected (figure 4.1).

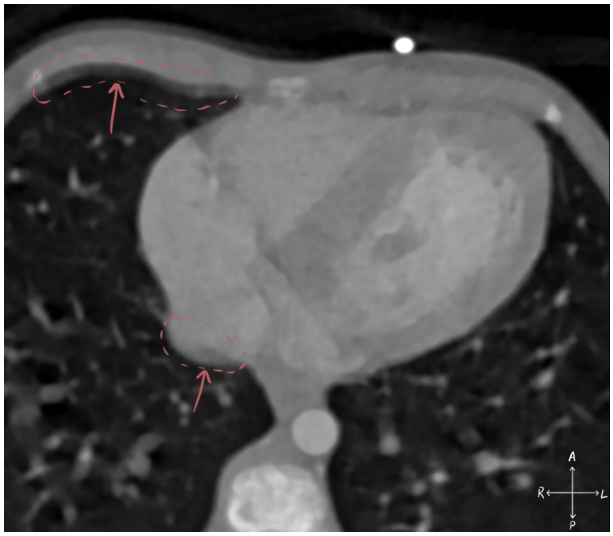

Figure 4.1: CT scan of the heart of the patient with KD. It shows superimposed features on a portion of the scan (pink circles and arrows). Axial view at the level of the inferior vena cava.

4.1.1 Segmented models

Considering that the visualisation of the coronary arteries were the main goal of this CT, this segmentation prioritised the proper display of the coronary arteries. The other substructures of the heart are normal, therefore a basic division in left and right heart will suffice.

Consequently, there are five segments: right heart, that encompasses the venae cavae, the pul-

monary artery, right atria and the right ventricle; left heart, that includes the ascending and descending aorta, the left atria and left ventricle; RCA - the right coronary is the most anterior of the coronary arteries and goes between the right atria and the right ventricle; LAD/LCX - the left coronary passes between the pulmonary trunk and the left auricle, and then divides into the anterior descending branch and the circumflex branch; and soft tissue, that is composed by the cardiac muscle that surrounds the aforementioned structures.

The thresholding method was used to generate the 3D representation of each of the segments. As there was a overlap of a few structures and a few defects in the segmentation, manual editing was made in order to correct and eliminate these mistakes. Once the segmentation was finished, the median smoothing effect was applied so that the boundaries of each segment become smoother, remove extrusions and fill small holes.

Two types of models were created: one hollow model in which only the soft tissue is present and the heart's internal structures are not present (figures 4.2 and 4.3); and other model made up by the major internal structures of the heart including the coronary arteries (figure 4.4).

The hollow model has a two-fold purpose as it acts as a visual indicator of the heart's outline and can be used for dosimetric studies by placing suitable dosimeters inside the model in the hollowed parts. This model was sectioned in two parts according to a transversal plane in order to have physical access to the hollowed parts and for the printing to be easier as the model has a flat surface thus reducing the amount of supports printed (figures 4.2b and 4.3a).

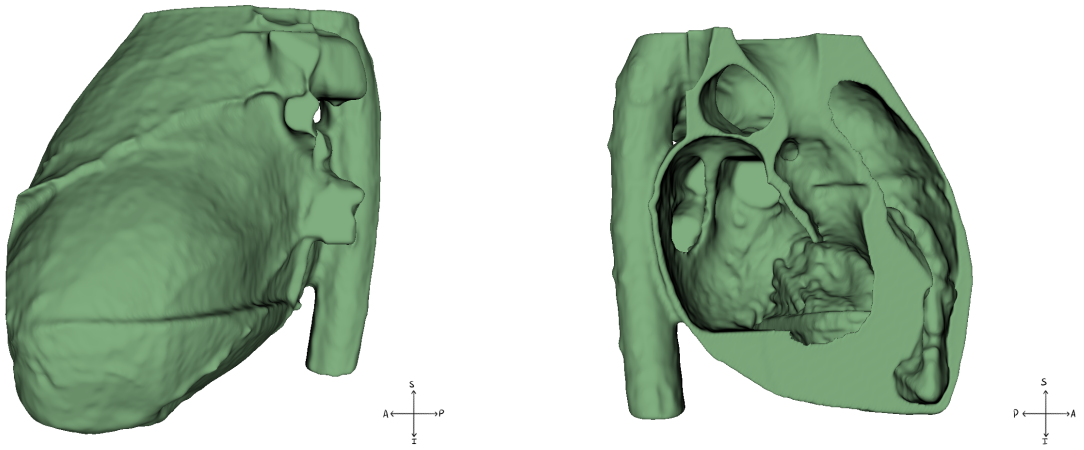

(a) Left view.

(b) Right view.

Figure 4.2: Result of the segmentation made with the CT scan of the heart of the patient with KD. Left section of the hollow model where the green structure represents the soft tissue.

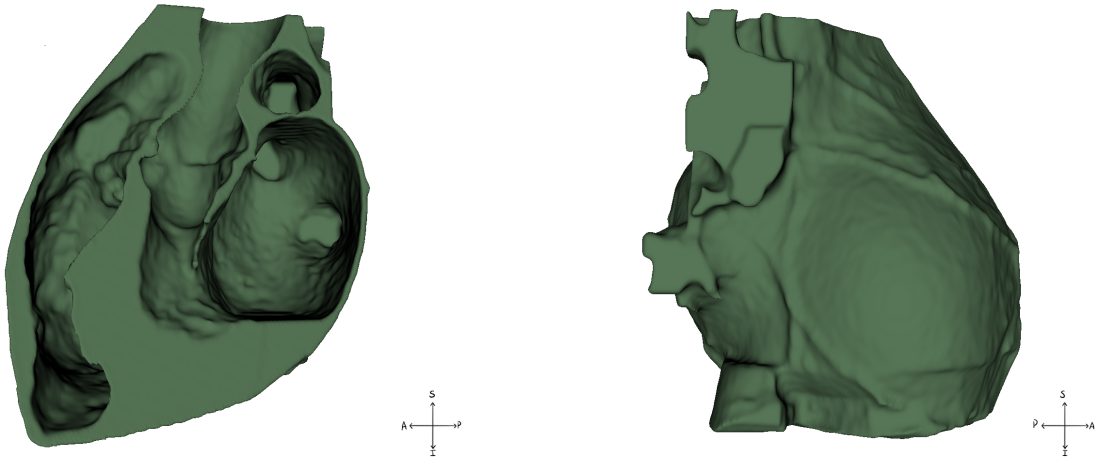

(a) Left view.

(b) Right view.

Figure 4.3: Result of the segmentation made with the CT scan of the heart of the patient with KD. Right section of the hollow model where the green structure represents the soft tissue.

In accordance with the hollow model, the blood-pool was sectioned following the same transversal plane (figure 4.4). This plane was chosen in a way to not cut through the coronary arteries segments for it to be accurately displayed and printed.

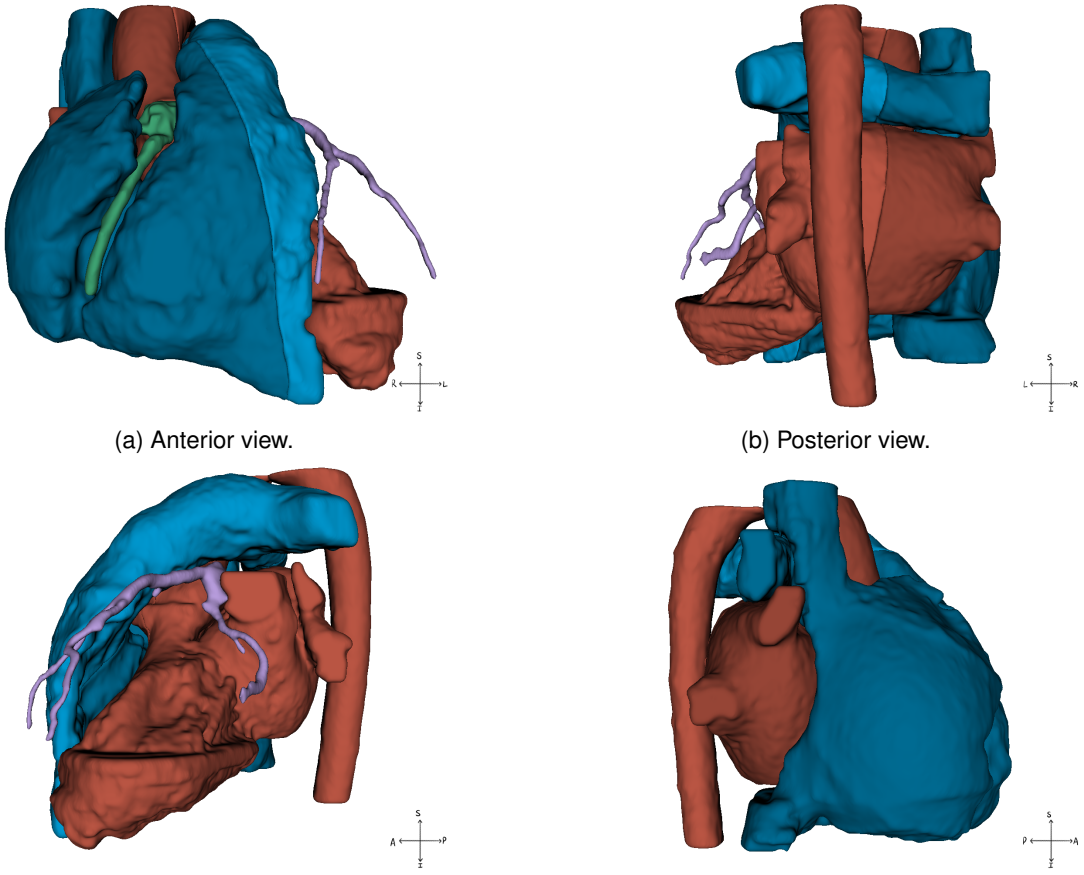

(a) Anterior view.

(b) Posterior view.

(c) Left view.

(d) Right view.

Figure 4.4: Result of the segmentation made with the CT scan of the heart of the patient with KD. Model of the blood-pool where the red illustrates the left heart, the blue depicts the right heart, the purple represents the left coronary artery, and the green displays the right coronary artery.

The main difficulties in the segmentation process of the heart of the patient with KD were to manually solve the errors created by the thresholding process, for instance, separate structures that had similar greyscale values but were not supposed to be nested together or having virtually no difference between the cardiac tissue and the diaphragm and having to manually produce an accurate inferior part of the soft tissue segment; decide the best location to cut vasculature namely the ramifications of the pulmonary artery and the pulmonary veins; reinforce the robustness and fix the openings in the hollow model caused by smoothing or by the subtraction of the internal structures.

4.1.2 Printed models

Overall, the hollow model had a suitable printing quality where the outline of the heart is easy to perceive, consequence of the high detail achieved in the imaging acquisition process (figures 4.5 and 4.6). Moreover, the inner hollowed out parts have detailed features, a repercussion of the high quality blood-pool segments that were subtracted to obtain the hollow model.

In order to maintain the structural stability of the hollow model, many supports were required. There were a few supports that could not be removed as they were in odd angles, in unreachable positions and the lack of adequate tools.

(a) Left view.

(b) Right view.

Figure 4.5: Result of the printing of the left section of the hollow model made with the CT scan of the heart of the patient with KD.

(a) Left view. (b) Right view.

Figure 4.6: Result of the printing of the right section of the hollow model made with the CT scan of the heart of the patient with KD.

The left heart segments had a fine printing quality with great details alike the ones created in the segmentation process. During the removal of the supports and handling the model, the descending aorta broke from the model (figure 4.7); the beginning of the aortic arch only had a few layers of material printed thus being fragile and would most likely break.

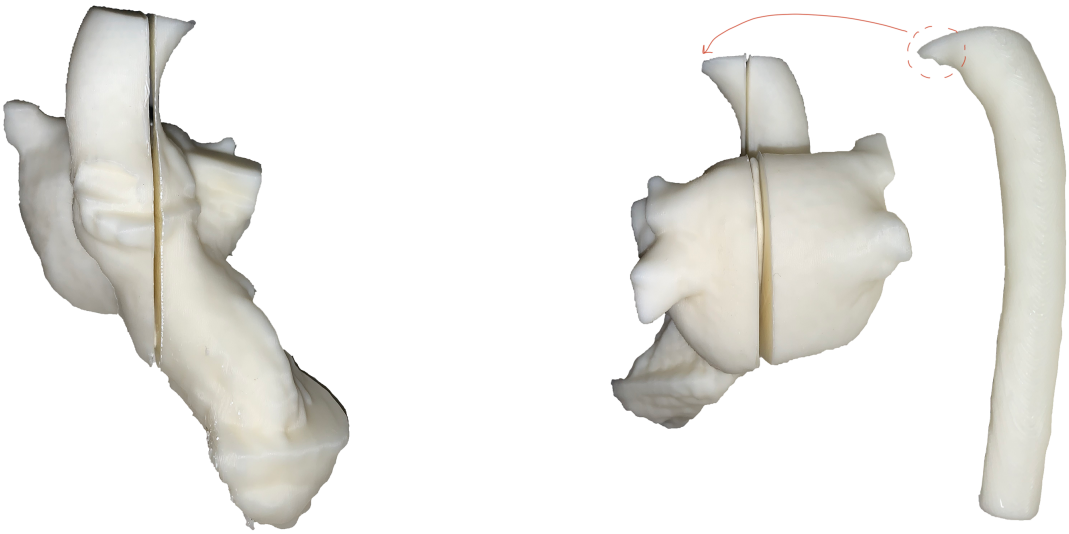

(a) Anterior view. (b) Posterior view.

Figure 4.7: Result of the printing of the left heart segment made with the CT scan of the heart of the patient with KD. Note the sectioned segments. A piece of the descending aorta fractured in the arch and, the red circle and arrow show where the fragment should be.

The right heart segments also showed an adequate printing quality with accurate features (figure 4.8).

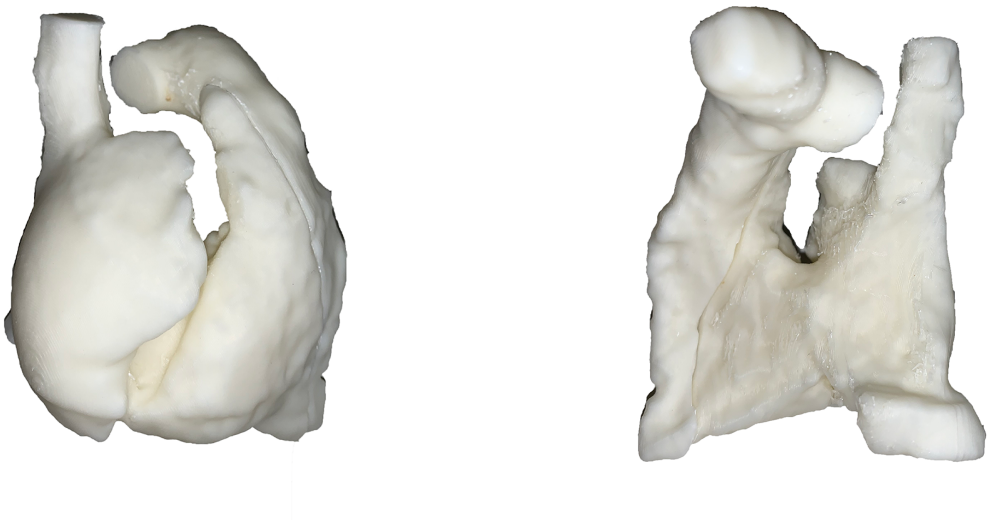

(a) Anterior view.

(b) Posterior view.

Figure 4.8: Result of the printing of the right heart segment made with the CT scan of the heart of the patient with KD. Note the sectioned segments.

Due to the fineness and fragility of the models, both were printed using the SLA printing methodology and the FDM method. The coronary arteries segments printed using the SLA method displayed an excellent printing quality with extremely precise features (figure 4.9). Unsurprisingly, a small portion shattered while removing the supports. Notwithstanding the fractured portion, the model maintained its accuracy.

(a) Left coronary artery.

(b) Right coronary artery.

Figure 4.9: Result of the printing of the coronary arteries segments made with the CT scan of the heart of the patient with KD. The red models were printed using the SLA printing method and the white models were printed using the FDM method.

4.1.3 Feedback

Overall, the medical doctors highlighted the absence of errors of segmentation and the printed models accurately replicated the anatomy of the patient's heart. The coronary arteries segments were praised by the excellent segmentation and printing work, being a faithful representation of the main issue in this case.

However, it was stressed the inconvenience of handling two sections of the same segment. A recommendation was made to refrain from sectioning the blood-pool segments as it is easier to feel and evaluate an intact model.

4.2 Case 2 - Tetralogy of Fallot

4.2.1 Segment definition

Bearing in mind the aforementioned defects present in this case, the division of left and right heart will serve to properly illustrate this patient's heart since these defects will be visible.

Thus, there are three segments: right heart, that encompasses the venae cavae, the pulmonary artery, right atria and the right ventricle; left heart, that includes the ascending and descending aorta, the left atria and left ventricle; and soft tissue, that is composed by the cardiac muscle that surrounds the aforementioned structures.

Similarly to the first case, the thresholding method was used to create a 3D rendering of the heart. Since some segments coincided, and there were defects in the segmentation, it was necessary to recur to manual editing so those major flaws could be corrected. Lastly, when all considerable errors were emended, a smoothing effect was applied to produce a smoother outcome and to remove any kind of extrusions or holes.

4.2.2 CT scan models

The CT scan of the heart of the patient with ToF had great quality, with a clear distinction between different types of tissues, and sharp definition of structures. There were not any visible artifacts on the scan.

Two types of models were created: one hollow model in which only the soft tissue is present that acts as a visual indicator of the heart's contour and can be used in dosimetric studies (figures 4.10 and 4.11); and other model made up by the major internal structures of the heart that serves as a standard for identifying the anomalies present in the structures (figure 4.12).

The hollow model was sectioned in two parts according to a transversal plane in order to have physical access to the hollowed parts and for the printing to be easier, as the model has a flat surface, thus reducing the amount of supports printed (figures 4.10b and 4.11a).

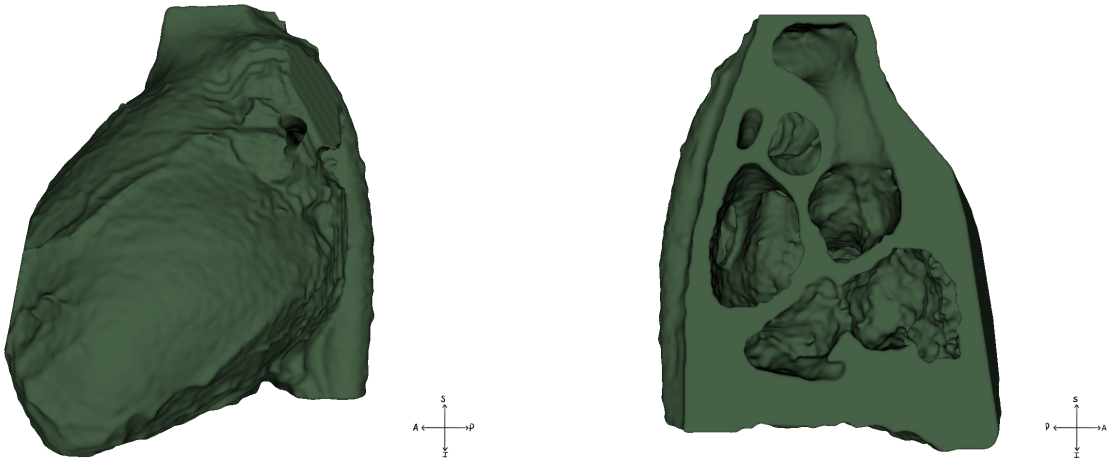

(a) Left view. (b) Right view.

Figure 4.10: Result of the segmentation made with the CT scan of the heart of the patient with ToF. Left section of the hollow model where the green structure represents the soft tissue.

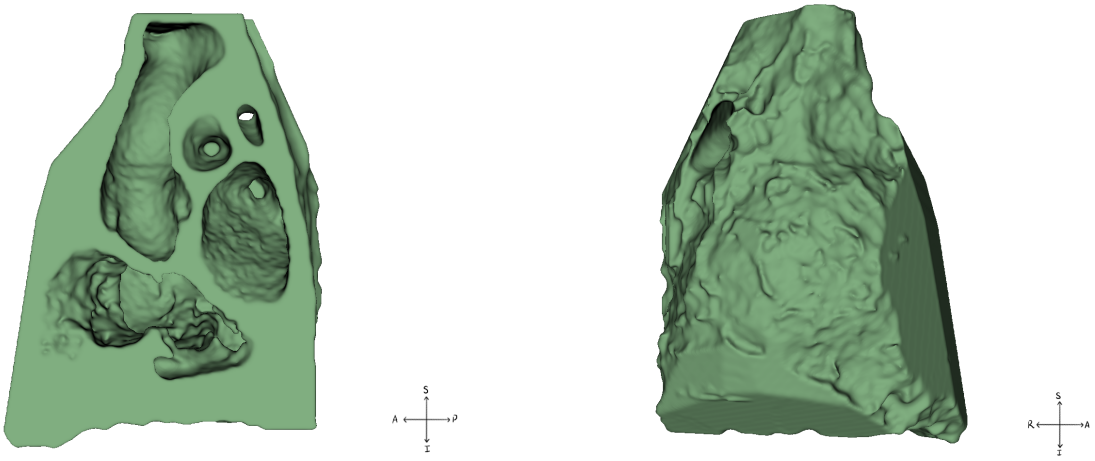

(a) Left view. (b) Right view.

Figure 4.11: Result of the segmentation made with the CT scan of the heart of the patient with ToF. Right section of the hollow model where the green structure represents the soft tissue.

Differently to the first case and following the reflections on sections 4.1.2 and 4.1.3, the internal structures were not sectioned in order to maintain structural integrity being easier to handle and to manage.

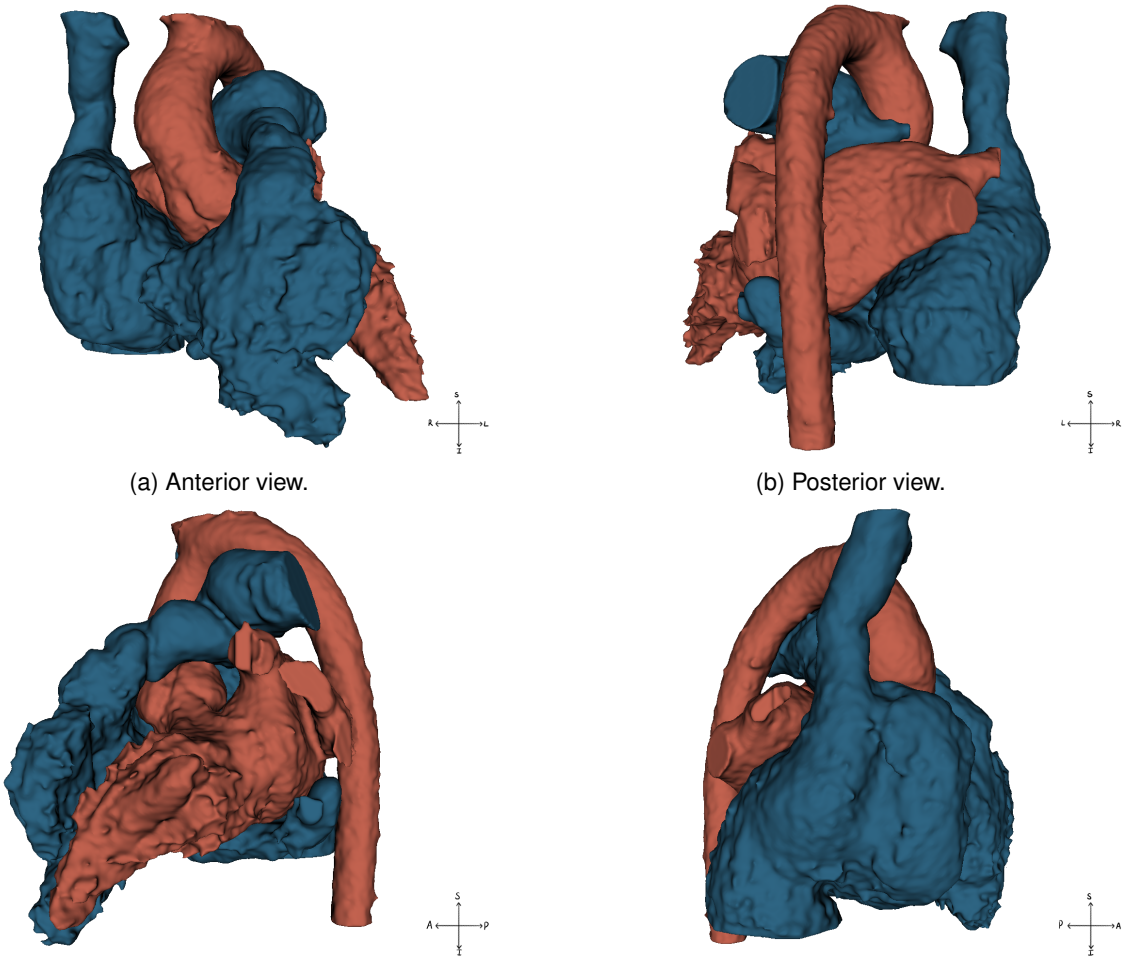

(a) Anterior view.

(b) Posterior view.

(c) Left view.

(d) Right view.

Figure 4.12: Result of the segmentation made with the CT scan of the heart of the patient with ToF. Blood-pool model where the red illustrates the left heart, and the blue depicts the right heart.

Some hurdles presented themselves in the segmentation process, such as accurately splitting up structures that were not supposed to be embedded together; trying to distinguish the cardiac tissue from the diaphragm and manually create the inferior part of the enclosure of the heart; deciding whether or not to smooth out the features of the segments to produce a more visually appealing model; and to try to strengthen the structural integrity of the hollow model after the subtraction of the internal structures.

4.2.2.1 Printed models

Generally, the hollow model had a good printing quality where the outline of the heart is easy to perceive, consequence of the high detail of the CT scan (figures 4.13 and 4.14). Furthermore, it is clear that the hollowed parts have quite thorough characteristics result of the subtraction of the internal structures (figure 4.14a).

As a consequence of the intricacies of the hollow model, a large amount of supports were necessary to aid the printing process and for the structural stability of the model. Unfortunately, there were some supports that could not be removed from the model since they were in strange angles, unreachable positions and the lack of adequate tools for removal (figure 4.13b).

(a) Left view.

(b) Right view.

Figure 4.13: Result of the printing of the left section of the hollow model made with the CT scan of the heart of the patient with ToF. The green circles highlight the supports that could not be removed.

(a) Left view.

(b) Right view.

Figure 4.14: Result of the printing of the right section of the hollow model made with the CT scan of the heart of the patient with ToF.

The left heart segment had a decent printing quality and presented fine details similar to the ones created in the segmentation process. While removing some of the supports, a part of the descending aorta fractured from the main model (figure 4.15). Considering that the descending aorta was practically supporting itself it came as no surprise when it fractured. One solution to this issue would be to increase the amount of infill on the descending aorta to reinforce the structure.

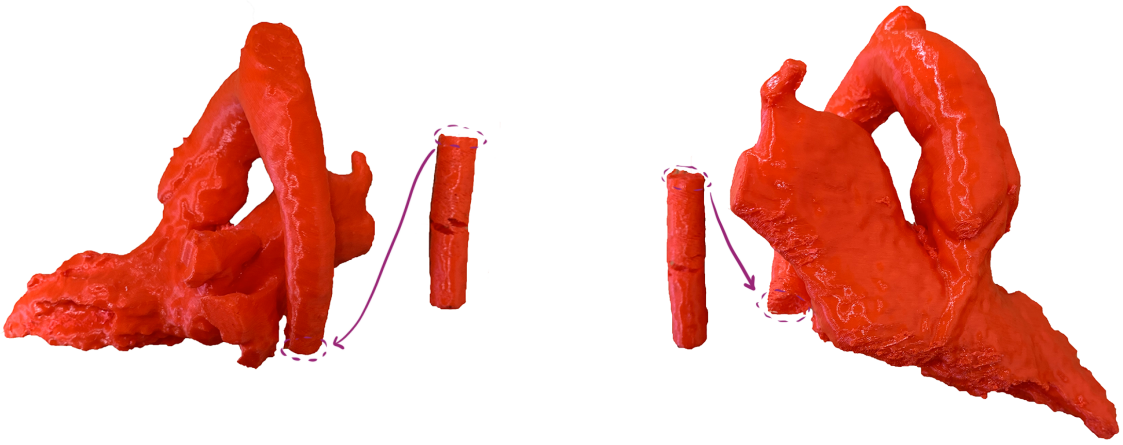

(a) Left view.

(b) Right view.

Figure 4.15: Result of the printing of the left heart segment made with the CT scan of the heart of the patient with ToF. A piece of the descending aorta fractured and, the purple circles and arrow show where the fragment should be.

The right heart segment also presented a satisfactory printing quality with precise features. Similar to the left heart segment, a piece of the model - the superior vena cava - broke by removal of the supports (figure 4.16). Again, if possible, these types of pieces should have more material printed to improve robustness and decrease the likeness of fractures in the model.

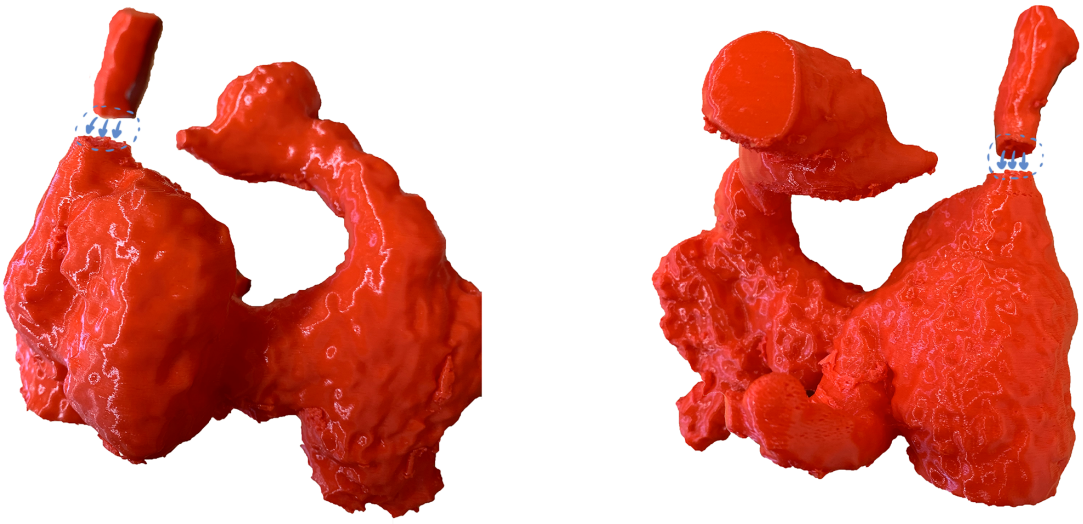

(a) Anterior view.

(b) Posterior view.

Figure 4.16: Result of the printing of the right heart segment made with the CT scan of the heart of the patient with ToF. A piece of the superior vena cava fractured and, the blue circle and arrows show where the fragment should be.

4.2.2.2 Feedback

In regards to the blood-pool models, the physicians emphasised the good quality of segmentation and the precision of anatomical replication. Yet, it was stated that the boundaries of the hollow models were primitive and did not portray correctly the outline of the cardiac tissue. The incorrect shape of certain parts in the hollow models - the flat portions visible in figure 4.14b - is a segmentation error , effect of the inability to distinguish certain portions of cardiac tissue and other tissues thus having to manually carve out the boundaries of the hollow model.

4.2.3 MRI scan models

The MRI scan of the heart of the patient with ToF had an overall appropriate image quality, with a good distinction between different types of tissues, a decent contrast between the soft tissue and the surrounding features and a satisfactory definition of the heart's structures. There is a large artifact present throughout the entirety of the scan that blocks part of the soft tissue, possibly affecting the segmentation process and producing an inconsistent model with reality (figure 4.17). This artifact is the result of the interaction between the multiple magnetic fields required to perform the MRI scan and the stainless steel wires that are used to close the sternum after cardiac surgery.

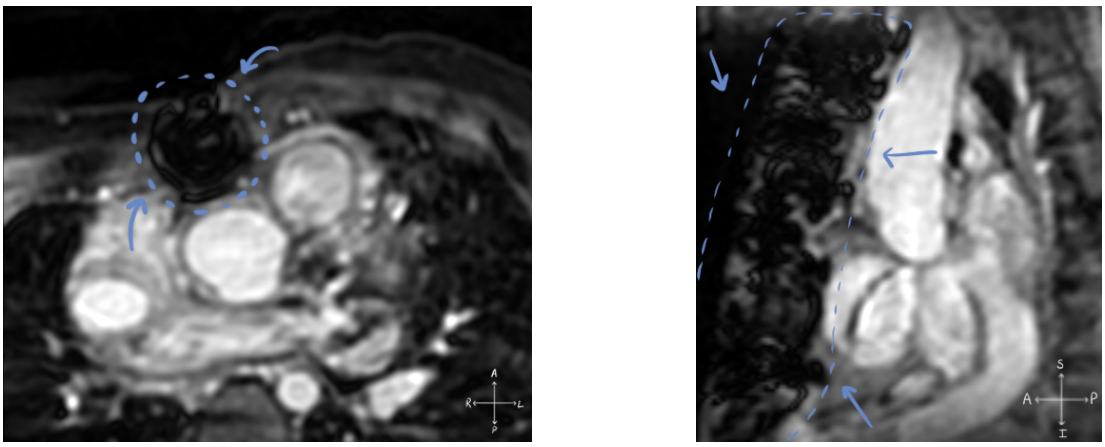

(a) Axial view.

(b) Sagittal view.

Figure 4.17: MRI scan of the heart of the patient with ToF. It exhibits large artifacts (blue circles and arrows) that might affect the outcome.

Again, two types of models were created: one hollow where the only existing segment is the soft tissue one and represents the heart's shape(figures 4.19 and 4.20); and other constituted by the main structures of the heart allowing to easily spot the defects present in the heart (figure 4.18).

Additionally, the hollow model was sectioned in two parts through a transversal plane so that one can access to the hollowed parts. Moreover, this eases the printing process since the model has a flat surface, consequently reducing the printing time and the amount of supports (figures 4.19b and 4.20a).

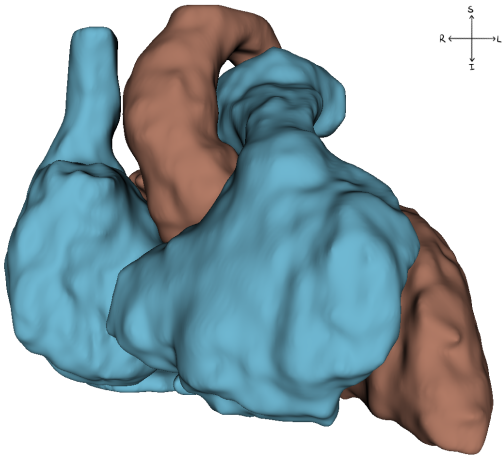

(a) Anterior view.

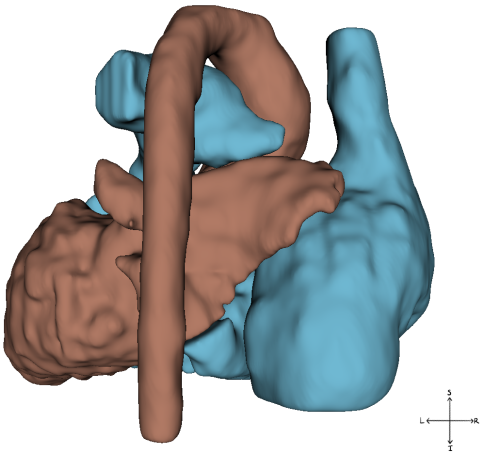

(b) Posterior view.

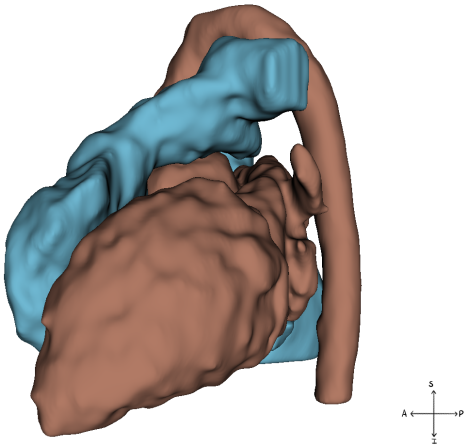

(c) Left view.

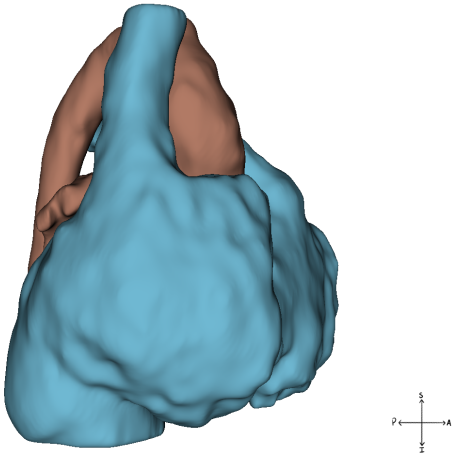

(d) Right view.

Figure 4.18: Result of the segmentation made with the MRI scan of the heart of the patient with ToF. Blood-pool model where the red represents the left heart, and the blue portrays the right heart.

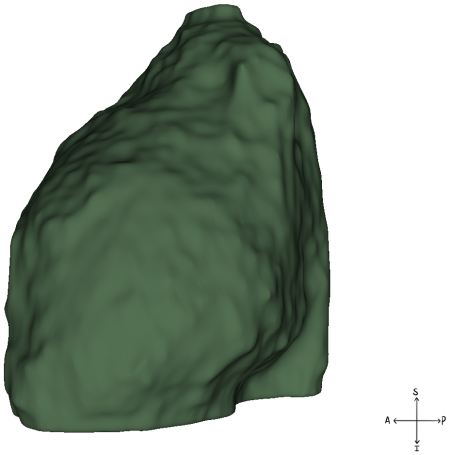

(a) Left view.

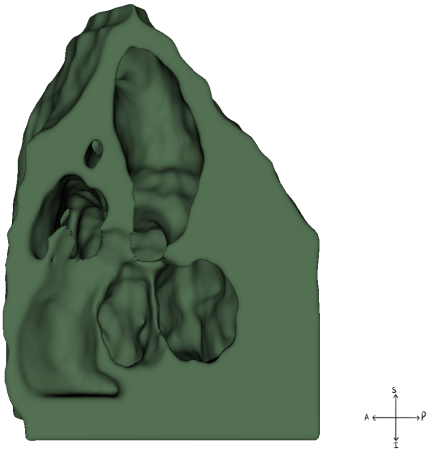

(b) Right view.

Figure 4.19: Result of the segmentation made with the MRI scan of the heart of the patient with ToF. Left section of the hollow model where the green structure represents the soft tissue.

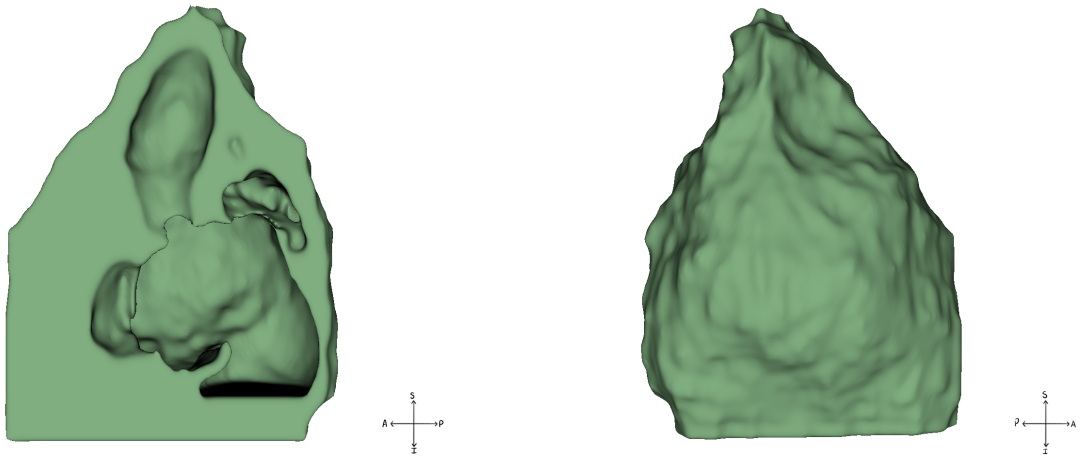

(a) Left view.

(b) Right view.

Figure 4.20: Result of the segmentation made with the MRI scan of the heart of the patient with ToF. Right section of the hollow model where the green structure represents the soft tissue.

As expected, the artifact in the MRI scan (figure 4.17) was an issue in the segmentation process. Manual editing was necessary to not only solve this matter but to work out a solution to the transversal issue of distinguishing the cardiac tissue from the diaphragm and design an anatomically accurate inferior part of the heart. In addition, fortifying the hollow model after the subtraction of the internal structures also caused a nuisance in the segmentation process.

4.2.3.1 Printed models

Because of time constrictions, the hollow model made with the MRI scan of the heart of the patient with ToF could not be printed.

The left heart segment displayed a satisfactory printing quality with reasonable details, consequence of the type of imaging acquisition technique and the segmentation. By having smoother edges, less supports were necessary in the printing process leading to no shattering pieces (figure 4.21).

(a) Anterior view.

(b) Posterior view.

Figure 4.21: Result of the printing of the left heart segment made with the MRI scan of the heart of the patient with ToF.

Correspondingly, the right heart segment presented as well an adequate printing quality with appropriate features (figure 4.22). Again, the reduced necessity of supports, result of the smoothness of the boundaries, in the printing process made it easier to keep the model intact with no fragmented pieces.

(a) Anterior view.

(b) Posterior view.

Figure 4.22: Result of the printing of the right heart segment made with the MRI scan of the heart of the patient with ToF.

However, owing to the smoothness of the final products, it is not certain that the printed models will have enough detail for an appropriate medical evaluation.

4.2.3.2 Feedback

Correspondingly, the blood-pool models that were made using the MRI data also presented a suitable quality of segmentation and printing. Even though the resulting models were smoothed out, it did not affect the medical evaluation.

4.3 Case 3 - Complex congenital heart disease

The MRI scan of the heart of the patient with complex CHD had a below average image quality, with a sufficient distinction between different types of tissues, a satisfactory contrast between the soft tissue and the surrounding features and a reasonable definition of the heart's structures. The MRI scan cut a small portion of the heart in the acquisition process and it might have consequences in the segmentation process.

Additionally, there are two types of large artifacts present throughout the entirety of the scan that block a large portion of the soft tissue and of the heart's structures. This might have a negative impact in the segmentation process further creating a different outcome (figure 4.23).

Similarly to the previous case, one type of the artifacts are the result of the interaction between the magnetic fields and the stainless steel wires employed to close the sternum after open-heart surgery.

Furthermore, the other type of artifacts comes from the interaction between the magnetic fields and a metallic prosthesis placed between the right ventricle and, the left ventricle and the only atrium.

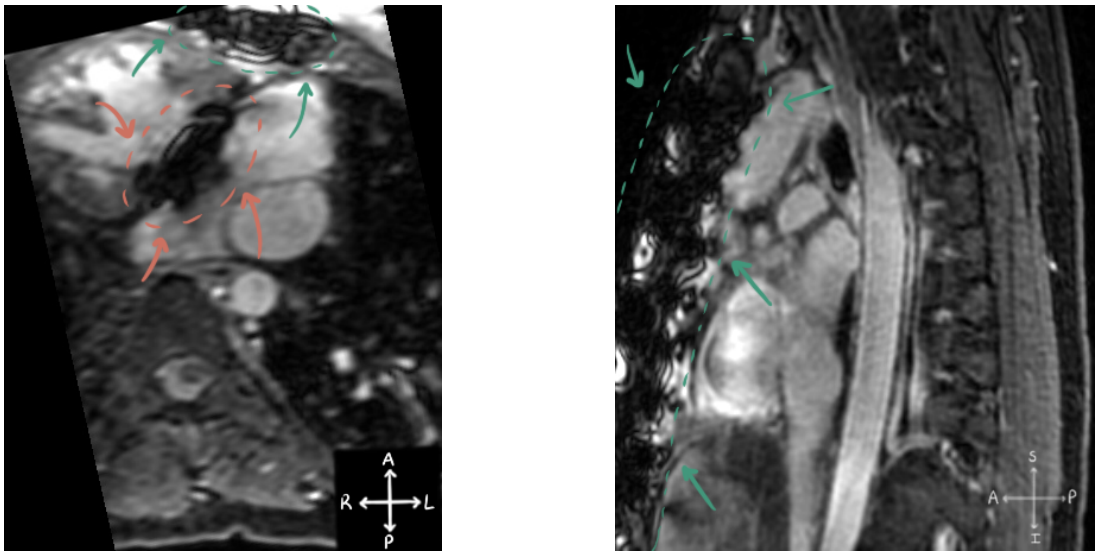

(a) Axial view.

(b) Sagittal view.

Figure 4.23: MRI scan of the heart of the patient with complex CHD. It exhibits large artifacts, that might affect the outcome, caused by the interaction of the magnetic fields, and the stainless steel wires used to close the sternum (green circle and arrows) and an metallic prosthesis (pink circle and arrows).

4.3.1 Segmented models

In view of the complexity of the case, it was decided that it would be easier to see the heart's structures as a whole. Hence, there are two segments: heart, that encompasses all the structures of the heart; and soft tissue, that is composed by the cardiac muscle that surrounds the aforementioned structures.

Once more, two types of models were created: one comprised of the structures of the heart (figure 4.26); another one that is hollow, where the only existing segment is the soft tissue one that outlines the heart (figures 4.24 and 4.25).

Furthermore, the hollow model was sectioned in two parts through a transversal plane. This aids and facilitates the printing process since the model has a flat surface, consequently reducing the printing time and the amount of supports (figures 4.24b and 4.25a).

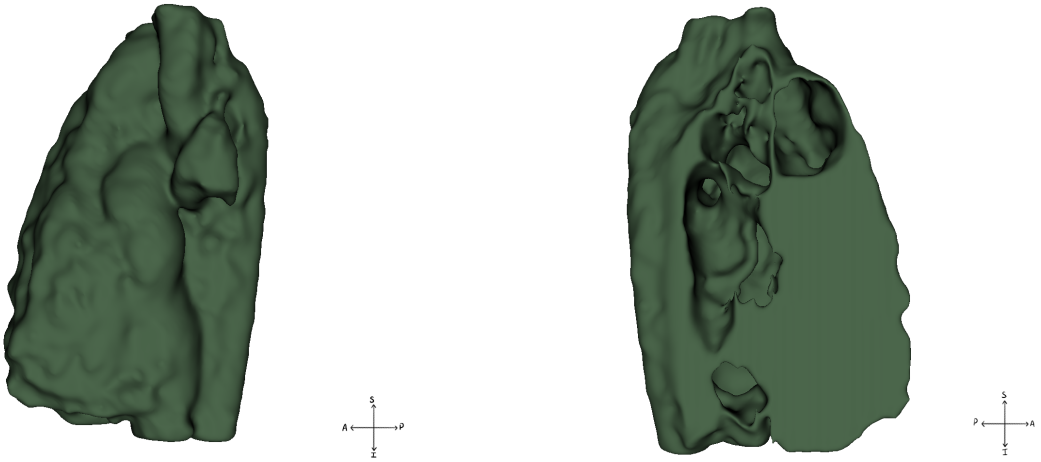

(a) Left view. (b) Right view.

Figure 4.24: Result of the segmentation made with the MRI scan of the heart of the patient with complex CHD. Left section of the hollow model where the green structure represents the soft tissue.

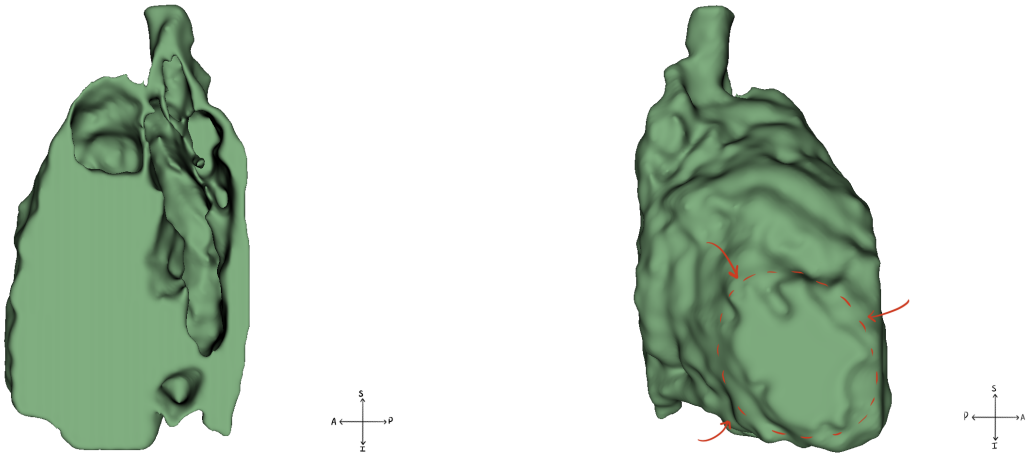

(a) Left view. (b) Right view.

Figure 4.25: Result of the segmentation made with the MRI scan of the heart of the patient with complex CHD. Right section of the hollow model where the green structure represents the soft tissue. The red circle and arrows highlight the flat surface consequence of part of the heart being cut off in the acquisition process.

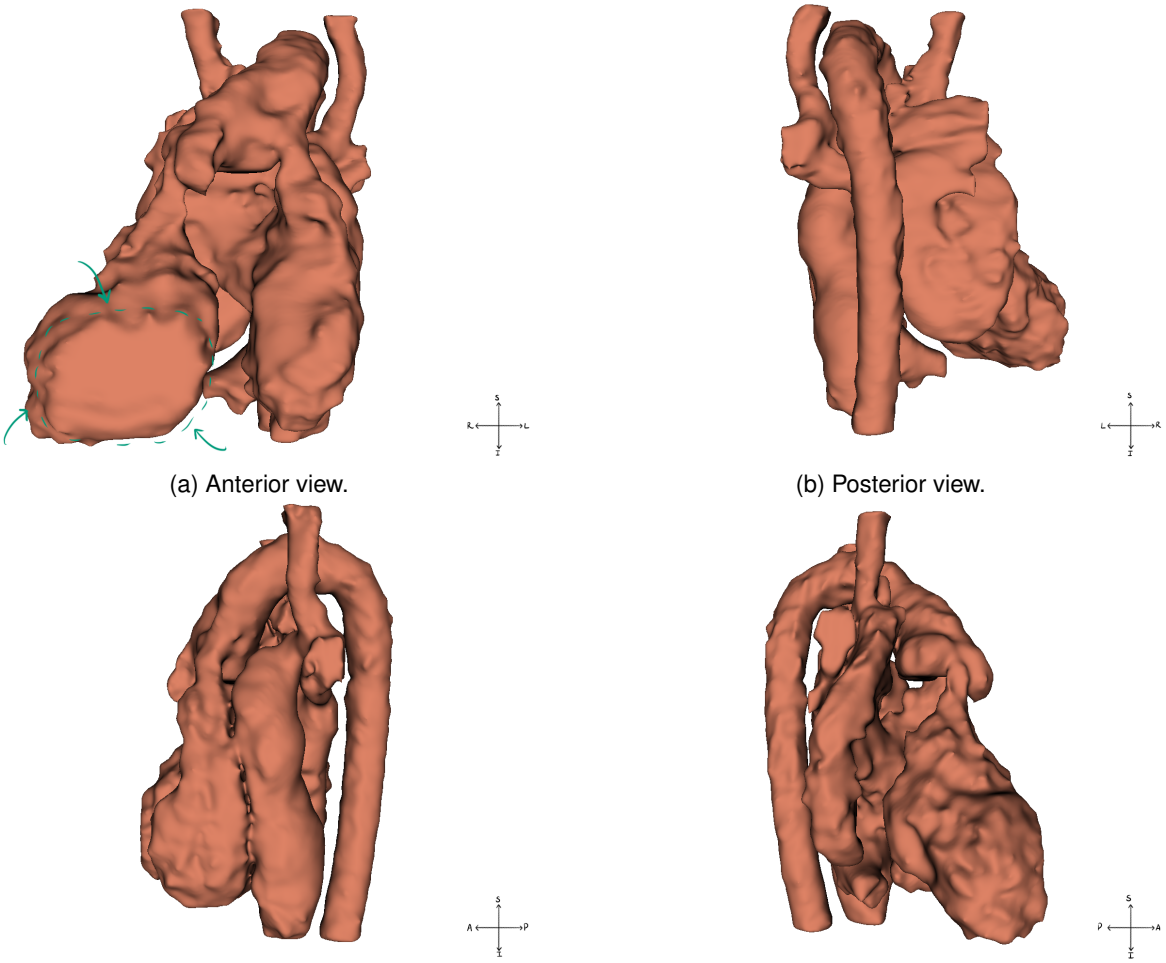

(a) Anterior view.

(b) Posterior view.

(c) Left view.

(d) Right view.

Figure 4.26: Result of the segmentation made with the MRI scan of the heart of the patient with complex CHD. Blood-pool model. The green circle and arrows in the anterior view emphasises the flat surface created as a repercussion of a portion of heart being divided in the acquisition process.

As it was foreseeable, the large artifact present in the MRI scan (figure 4.23) revealed itself as a major issue in the segmentation process. In order to work out this matter, manual editing was once again necessary. As it was stated previously, part of the heart was cut in the acquisition process causing a part of the segmentation to be flat (visible in figures 4.25b and 4.26a). On account of the complexity of the case and the poor quality of the MRI scan, it became difficult to comprehend what was a heart structure and what was not, making the segmentation process more troublesome.

4.3.2 Printed models

In general, the hollow model presented a reasonable printing quality with subpar features, an effect caused by the resolution of the MRI (figures 4.27 and 4.28). Nevertheless, the viewer can easily make out the enclosure of the heart just by looking to the model. In addition, a few of the supports could not be removed, an effect of supports in odd angles, in unattainable locations and the absence of adequate tools for removal (figure 4.27b).

(a) Left view. (b) Right view.

Figure 4.27: Result of the printing of the left section of the hollow model made with the MRI scan of the heart of the patient with complex CHD. The green circles accentuate the supports that could not be removed.

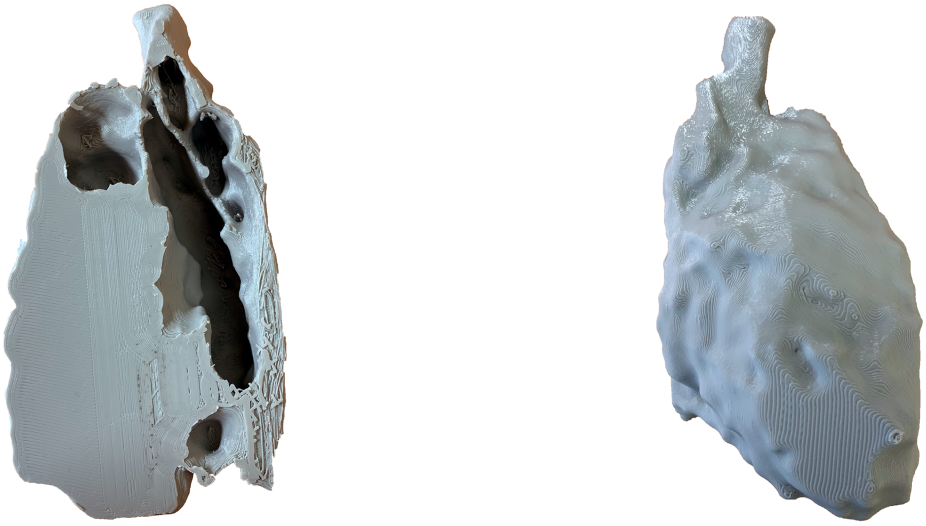

(a) Left view. (b) Right view.

Figure 4.28: Result of the printing of the right section of the hollow model made with the MRI scan of the heart of the patient with complex CHD.

Lastly, the heart segment had an acceptable printing quality with mediocre details, product of the complexity of the case and the image acquisition technique (figure 4.29). Predictably, a few pieces fractured while handling and trying to remove the supports from the model namely a part of the descending aorta, one of the superior venae cavae and the only ventricle that fractured in the unique atrioventricular valve (figure 4.29a). Furthermore, as was highlighted earlier, more material should be printed onto these fragile areas to ensure structural stability.

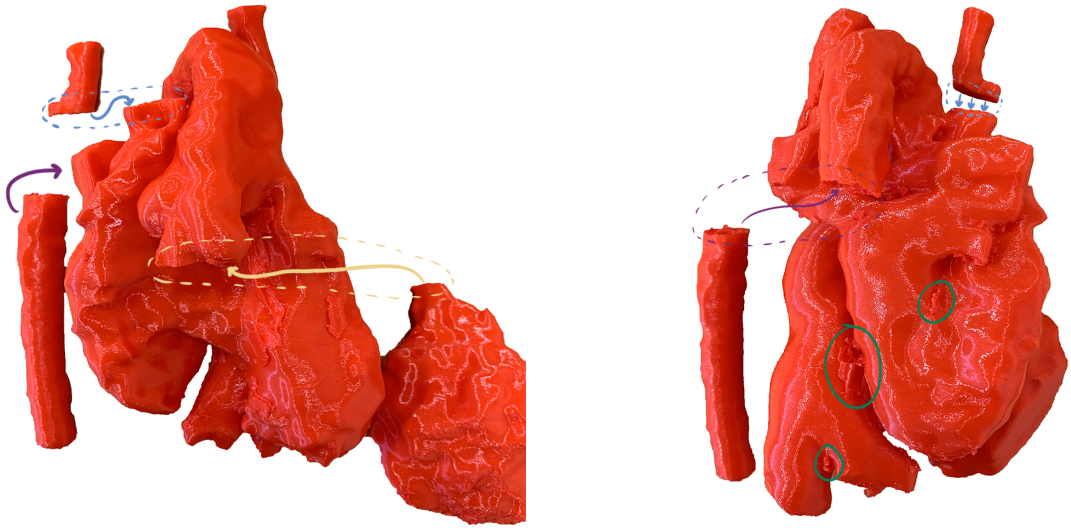

(a) Anterior view.

(b) Posterior view.

Figure 4.29: Result of the printing of the heart segment made with the MRI scan of the heart of the patient with complex CHD. There were three pieces of the model that fractured; the drawings show where the piece should be: one of the superior venae cavae represented by the blue circle and arrow; the descending aorta illustrated by the purple arrows and circle; and the only ventricle characterised by the yellow arrow and circle. The green circles emphasise the structures that could not be removed.

4.3.3 Feedback

In contrast to the hollow models made using CT data of the previous case, the hollow models accurately reproduced the cardiac tissue that surrounds the heart's structure as a result of the superior soft tissue contrast that a MRI scan can provide.

The medical doctors pointed out several faults and inaccuracies in the printed model consequence of the segmentation process. In the segmentation the right superior vena cava is both attached to the atrium and to the pulmonary artery when its only connection should be the pulmonary artery. Furthermore, part of the interventricular septum was prolonged, not showing the communication between the left and right ventricles. These mistakes can be attributed to the poor quality of the MRI scan and the complexity of the case. Despite these slip-ups, other key structures were properly segmented such as the fenestra, a small opening between the atrium and the left ventricle.

4.4 Dosimetry studies

One of the most interesting applications of the 3D printed models is dosimetry. Since patients with CHD are subject to radiation exposure diagnosis methods like CT, chest X-ray and intervention radiology from early ages until adulthood, it is paramount to have an accurate estimation of the dose received in each exam. This issue has been flagged by the European Commission as a major question to be solved.

By creating a realistic hollow model, accurate measurements that take into account each patient's unique anatomy to estimate the dose can be made by performing a detailed dose distribution in the personalised organ using appropriate dosimeters such as thermoluminescent dosimeters (TLDs). Fur-

thermore, this kind of study can provide insightful data in order to optimise the CT parameters regarding dose in neonates and children.

Unfortunately, due to the COVID-19 pandemic, this study could not be made as restrictions were imposed and the access to the hospital was restricted to medical emergencies only. All printed models are functional and ready to be used to obtain the objective that was initially proposed.

Chapter 5

Discussion and Conclusions

Generally speaking, each imaging method has its advantages and disadvantages when it comes to create and print a 3D model based on the data of each scan. A CT scan has a superior spatial resolution and is a fairly quick, however, it has lower sensitivity and has the increased risk of radiation exposure [48]. A MRI scan has high sensitivity, a good soft tissue contrast, the possibility of performing functional studies and, low risk of radiation exposure, yet, it has a slow scanning speed and it has a high chance of having inevitable artifacts consequence of metallic structures [48]. Bearing this in mind, an adequate equilibrium between these two imaging methods can be met considering they complement each other.

Naturally, this study had several limitations in the segmentation and printing process.

In the segmentation process, the artifacts in the MRI scans emerged as a major issue and its effects were only diminished and never fully corrected by manual editing, as well as the transversal issue of differentiating the cardiac tissue from the adjacent tissues, more evident on the segmentations that used CT data. Moreover, importing the MRI scans onto the segmentation software turned out a challenge since the most reliable sequences were not recognised in the software, causing interpolation issues and influencing the image quality and the model itself. A way around this matter would be to search and explore different kinds of software that accept these sequences to improve the segmentation quality.

In the printing process, while handling the model and removing some of the supports a few pieces fractured from the main model; a solution to this issue would be to increase the infill density on these fragile spots and if not possible on the whole model therefore increasing the sturdiness of the model but also increasing the printing time. Additionally, removing the supports from the hollow model revealed itself to be a difficult, strenuous and time consuming activity; not all of the supports could be removed.

Despite the fact that the hollow models certainly represent the unique anatomy of each patient, in order to have precise dosimetric measurements that lead to reliable estimations of dose, it is necessary to have models with comparable tissue densities to the cardiac tissue of 1.055 g/mL [49].

Most hollow models in this study were printed with PLA filament due to its low price, resistance to temperature and good mechanical properties [50].

The PLA filament has a density of about 1.25 g/cm^3 and the ABS filament with a density around 1.05 g/cm^3.

At first glance, the ABS filament might seem an excellent candidate to replicate the tissue attenuation. However, and having into account the infill density of the printed models, the overall density of the models decreases for both filaments consequence of the printing parameters, gaps with air, and contractions that might have happened after the cooling of the filament [51].

Therefore, the PLA filament would be the adequate choice for printing the models that accurately replicates the tissue attenuation.

Considering that the ABS filament has measurable hindrances such as the difficulty to maintain proper temperatures and the necessity of a closed printer, all the models can be printed using the PLA filament for an easier printing process.

5.1 Achievements

This thesis proposed to create 3D printed models of the hearts of children with heart disease using images from CT and MRI scans. To do so, the resulting files from the CT and MRI scans were imported into a segmentation software to separate the different regions of the heart and export these segments towards a format compatible with the 3D printer. After this, the files are imported into a slicing software for them to be printed. The final printed models were handled and evaluated by medical doctors.

Upon the analysis of medical doctors, it was concluded that the blood-pool models presented a detailed and meticulous representation of the heart's anatomy and, the hollow models exhibit an off-putting outcome in certain areas as a consequence of drawbacks in the segmentation process. In addition, the models were said to be adequate for surgical planning considering the appropriate representation of the heart's structures, and its role in comprehending, as a whole, the heart conditions.

This work managed to create 3D models that accurately represented the anatomy of hearts of children with heart disease. Furthermore, it accomplished to produce precise hollow models that can be used in dosimetric studies that considers the individual's unique anatomy and that can further aid the search for optimisation of CT parameters with regards to paediatric patients.

5.2 Future work

Nowadays, the use of 3D printing is limited to procedural planning or simple anatomical teaching. However, with the advances on this technology, the treatment of CHD could encompass patient-specific devices, for instance, homografts, shunts or prosthetic valves such as atrial septal defect (ASD) and ventricular septal defect (VSD) closure valves, and left atrial appendage (LAA) occlusion in order to decrease the frequency of post-procedural device failure and complications given that these devices are suited to each patient's unique anatomy [52].

One of the key elements on developing 3D printed models that can be used in cardiology is the capacity of reproducing with a high degree of accuracy the cardiac tissue and its anatomical properties. Besides, not sectioned hollow models can be used as a teaching tool to simulate interventional cardiology. This will improve the evaluation of the physiological consequences of defects and will better prepare

trainees for interventional procedures. With this is mind, it is paramount to realise that using this type of technology to plan complex surgical procedures or to develop custom-made devices demands a highly accurate model of the anatomical properties and minimal errors [52].

In order to achieve these requirements, the 3D printed models have to be printed with more flexible materials that resemble cardiac tissue and its functions. This poses an issue since native cardiac tissue has a lot of intricacies and properties that change over time and physiological state [52].

Additionally, as was previously mentioned, 3D printed models can also be used to obtain dosimetric measurements from ionising radiation procedures and to further advance dose-reduction. So, to secure measurements more accurate as possible, the 3D printed models have to be printed with materials that have similar radiodensities to the different tissues that compose a heart.

Therefore, and due to the novelty of the area of material exploration, research into materials with a wide range of malleability, than can closely mimic the mechanical and physiological properties of the cardiac tissue, and have resembling radiodensities is crucial and must continue [52]. Moreover, it is imperative that these types of material are affordable so that they do not hinder the progress of using the 3D printing technology in cardiology [1, 2, 29, 52]. Besides the innovative non-biological material research, bioprinting and molecular printing will be key factors in advancing the 3D printing technology. These methods consist on building tissues with complex structures that are biologically engineered thus mimicking cardiac tissue and structures. Yet, these techniques face the issue to create a tissue that is functional and viable [52].

In conclusion, 3D printing has the potential to make a profound transformation in cardiology towards personalised, meticulous and accurate medicine as the 3D printed models can improve the quality of treatment and provide important tools for decision making [52].

Bibliography

[1] M. Cantinotti, I. Valverde, and S. Kutty, "Three-dimensional printed models in congenital heart disease," *The international journal of cardiovascular imaging*, vol. 33, no. 1, pp. 137–144, 2017.

[2] S.-J. Yoo, O. Thabit, E. K. Kim, H. Ide, D. Yim, A. Dragulescu, M. Seed, L. Grosse-Wortmann, and G. van Arsdell, "3D printing in medicine of congenital heart diseases," *3D printing in medicine*, vol. 2, no. 1, p. 3, 2016.

[3] J. Ryan, J. Plasencia, R. Richardson, D. Velez, J. J. Nigro, S. Pophal, and D. Frakes, "3D printing for congenital heart disease: a single site's initial three-year experience," *3D printing in medicine*, vol. 4, no. 1, p. 10, 2018.

[4] H. Bosmans, J. Damilakis, H. D. le Pointe, S. J. Foley, and et al., "European Guidelines on Diagnostic Reference Levels for Paediatric Imaging," in *Radiation Protection Nº 185*. European Commission, 2018.

[5] G. Oliveira and J. Saraiva, *Lições de Pediatria Vol. I e II*. Coimbra: Imprensa da Universidade de Coimbra, 2017.

[6] K. Marcdante and R. Kliegman, *Nelson Essentials of Pediatrics*. Elsevier, 2018.

[7] H. D. Allen, D. J. Driscoll, R. E. Shaddy, and T. F. Feltes, *Moss & Adams' heart disease in infants, children, and adolescents: including the fetus and young adult*. Lippincott Williams & Wilkins, 2013.

[8] M. A. Gatzoulis, L. Swan, J. Therrien, and G. A. Pantely, *Adult congenital heart disease: a practical guide*. John Wiley & Sons, 2008.

[9] F. F. Pinto, S. Laranjo, M. Mota Carmo, M. J. Brito, and R. Cruz Ferreira, "Twelve years of Kawasaki disease in Portugal," *The Pediatric infectious disease journal*, vol. 36, no. 4, pp. 364–368, 2017.

[10] E. Opfer and S. Shah, "Advances in pediatric cardiovascular imaging," *Missouri medicine*, vol. 115, no. 4, p. 354, 2018.

[11] F. Bailliard, M. L. Hughes, and A. M. Taylor, "Introduction to cardiac imaging in infants and children: techniques, potential, and role in the imaging work-up of various cardiac malformations and other pediatric heart conditions," *European Journal of Radiology*, vol. 68, no. 2, pp. 191–198, 2008.

[12] L. Romans, *Computed Tomography for Technologists: A comprehensive text*. Lippincott Williams & Wilkins, 2011.

[13] E. Seeram, "Computed tomography: A technical review," *Radiologic technology*, vol. 89, no. 3, pp. 279CT–302CT, 2018.

[14] R. H. Anderson, E. J. Baker, A. Redington, M. L. Rigby, D. Penny, and G. Wernovsky, *Paediatric Cardiology*, 3rd ed. Churchill Livingstone, 2009.

[15] F. P. Chan, "MR and CT imaging of the pediatric patient with structural heart disease," in *Seminars in Thoracic and Cardiovascular Surgery: Pediatric Cardiac Surgery Annual*, vol. 12. Elsevier, 2009, pp. 99–105.

[16] ICRP, *ICRP publication 60: 1990 recommendations of the International Commission on Radiological Protection*. Elsevier Health Sciences, 1991, no. 60.

[17] J. Valentin, "International commission on radiological protection. the 2007 recommendations of the international commission on radiological protection," *Annals of the ICRP, ICRP Publication*, vol. 103, pp. 2–4, 2007.

[18] Z. Brady, F. Ramanauskas, T. Cain, and P. Johnston, "Assessment of paediatric ct dose indicators for the purpose of optimisation," *The British journal of radiology*, vol. 85, no. 1019, pp. 1488–1498, 2012.

[19] S. Cohen, A. Liu, M. Gurvitz, L. Guo, J. Therrien, C. Laprise, J. S. Kaufman, M. Abrahamowicz, and A. J. Marelli, "Exposure to low-dose ionizing radiation from cardiac procedures and malignancy risk in adults with congenital heart disease," *Circulation*, vol. 137, no. 13, pp. 1334–1345, 2018.

[20] R. Harbron, S. Dreuil, M. Bernier, M. Pearce, I. Thierry-Chef, C. Chapple, and H. Baysson, "Patient radiation doses in paediatric interventional cardiology procedures: a review," *Journal of Radiological Protection*, vol. 36, no. 4, p. R131, 2016.

[21] C. K. Rigsby, S. E. McKenney, K. D. Hill, A. Chelliah, A. J. Einstein, B. K. Han, J. D. Robinson, C. L. Sammet, T. C. Slesnick, and D. P. Frush, "Radiation dose management for pediatric cardiac computed tomography," *Pediatric radiology*, vol. 48, no. 1, pp. 5–20, 2018.

[22] P. C. Cevallos, A. K. Armstrong, A. C. Glatz, B. H. Goldstein, T. M. Gudausky, R. A. Leahy, C. J. Petit, S. Shahanavaz, S. M. Trucco, and L. J. Bergersen, "Radiation dose benchmarks in pediatric cardiac catheterization: a prospective multi-center c3po-qi study," *Catheterization and Cardiovascular Interventions*, vol. 90, no. 2, pp. 269–280, 2017.

[23] European Society of Radiology *et al.*, "Patient safety in medical imaging: A joint paper of the European Society of Radiology (ESR) and the European Federation of Radiographer Societies (EFRS)," *Insights into Imaging*, vol. 10, no. 1, p. 45, 2019.

[24] A. Karambatsakidou, A. Omar, A. Fransson, and G. Poludniowski, “Calculating organ and effective doses in paediatric interventional cardiac radiology based on dicom structured reports–is detailed examination data critical to dose estimates?” *Physica Medica*, vol. 57, pp. 17–24, 2019.

[25] R. Y. Kwong, M. Jerosch-Herold, and B. Heydari, *Cardiovascular magnetic resonance imaging*. Springer, 2018.

[26] R. W. Brown, Y.-C. N. Cheng, E. M. Haacke, M. R. Thompson, and R. Venkatesan, *Magnetic resonance imaging: physical principles and sequence design*. John Wiley & Sons, 2014.

[27] K. Coyne, “MRI: A Guided Tour,” 2020. [Online]. Available: https://nationalmaglab.org/education/magnet-academy/learn-the-basics/stories/mri-a-guided-tour

[28] V. Muthurangu, “Pediatric and congenital heart disease,” in *Protocols and Methodologies in Basic Science and Clinical Cardiac MRI*. Springer, 2018, pp. 385–397.

[29] M. Vukicevic, B. Mosadegh, J. K. Min, and S. H. Little, “Cardiac 3D printing and its future directions,” *JACC: Cardiovascular Imaging*, vol. 10, no. 2, pp. 171–184, 2017.

[30] S. Anwar, G. K. Singh, J. Miller, M. Sharma, P. Manning, J. J. Billadello, P. Eghtesady, and P. K. Woodard, “3D printing is a transformative technology in congenital heart disease,” *JACC: Basic to Translational Science*, vol. 3, no. 2, pp. 294–312, 2018.

[31] T. Bartel, A. Rivard, A. Jimenez, C. A. Mestres, and S. Müller, “Medical three-dimensional printing opens up new opportunities in cardiology and cardiac surgery,” *European heart journal*, vol. 39, no. 15, pp. 1246–1254, 2017.

[32] V. Tsapaki, “Radiation dose in interventional cardiology,” *Imaging in Medicine*, vol. 2, no. 3, pp. 303–312, 2010.

[33] D.-E. Chabner, “Medical terminology: A short course/by davi-ellen chabner,” 2015.

[34] F. Da Silva, “The role of r-spondin3 in coronary artery formation and novel roles for retinoic acid signaling in cardiac development and repair,” Ph.D. dissertation, Université Côte d’Azur, 2017.

[35] H. Gray, *Anatomy of the human body*. New York: Bartleby.com, 2000.

[36] “Heart,” 2020. [Online]. Available: https://www.amboss.com/us/knowledge/Heart

[37] A. C. Guyton and J. E. Hall, *Textbook of Medical Physiology*, 12th ed. Elsevier, 2011.

[38] P. Peng, K. Lekadir, A. Gooya, L. Shao, S. E. Petersen, and A. F. Frangi, “A review of heart chamber segmentation for structural and functional analysis using cardiac magnetic resonance imaging,” *Magnetic Resonance Materials in Physics, Biology and Medicine*, vol. 29, no. 2, pp. 155–195, 2016.

[39] R. Drake, W. Vogl, and A. Mitchell, *Gray’s Anatomy for Students*. Elsevier, 2019.

[40] X. Zhuang, “Challenges and methodologies of fully automatic whole heart segmentation: a review,” *Journal of healthcare engineering*, vol. 4, no. 3, pp. 371–407, 2013.

[41] X. Zhuang, “Automatic whole heart segmentation based on image registration,” Ph.D. dissertation, UCL (University College London), 2010.

[42] S. Pieper, M. Halle, and R. Kikinis, “3D Slicer,” in *2004: 2nd IEEE International Symposium on Biomedical Imaging: Nano to Macro (IEEE Cat No. 04EX821)*, 2004, pp. 632–635 Vol. 1.

[43] X. Zhuang, L. Li, C. Payer, D. Štern, M. Urschler, M. P. Heinrich, J. Oster, C. Wang, Ö. Smedby, C. Bian *et al.*, “Evaluation of algorithms for multi-modality whole heart segmentation: An open-access grand challenge,” *Medical image analysis*, vol. 58, p. 101537, 2019.

[44] O. S. Carneiro, A. Silva, and R. Gomes, “Fused deposition modeling with polypropylene,” *Materials & Design*, vol. 83, pp. 768–776, 2015.

[45] G. B. Kim, S. Lee, H. Kim, D. H. Yang, Y.-H. Kim, Y. S. Kyung, C.-S. Kim, S. H. Choi, B. J. Kim, H. Ha *et al.*, “Three-dimensional printing: basic principles and applications in medicine and radiology,” *Korean journal of radiology*, vol. 17, no. 2, pp. 182–197, 2016.

[46] S. Corbel, O. Dufaud, and T. Roques-Carmes, “Materials for stereolithography,” in *Stereolithography*. Springer, 2011, pp. 141–159.

[47] P. D. Maldjian and M. Saric, “Approach to dextrocardia in adults,” *American Journal of Roentgenology*, vol. 188, no. 6_supplement, pp. S39–S49, 2007.

[48] Z. Shaikh, A. Torres, and M. Takeoka, “Neuroimaging in pediatric epilepsy,” *Brain Sciences*, vol. 9, no. 8, p. 190, 2019.

[49] A. Fuchs, M. R. Mejdahl, J. T. Kühl, Z. R. Stisen, E. J. P. Nilsson, L. V. Køber, B. G. Nordestgaard, and K. F. Kofoed, “Normal values of left ventricular mass and cardiac chamber volumes assessed by 320-detector computed tomography angiography in the Copenhagen General Population Study,” *European Heart Journal-Cardiovascular Imaging*, vol. 17, no. 9, pp. 1009–1017, 2016.

[50] A. Rodríguez-Panes, J. Claver, and A. M. Camacho, “The influence of manufacturing parameters on the mechanical behaviour of PLA and ABS pieces manufactured by FDM: A comparative analysis,” *Materials*, vol. 11, no. 8, p. 1333, 2018.

[51] M. Savi, M. A. Andrade, and M. P. Potiens, “Commercial filament testing for use in 3d printed phantoms,” *Radiation Physics and Chemistry*, vol. 174, p. 108906, 2020.

[52] M. B. Elshazly and M. Hoosien, “The future of 3D printing in cardiovascular disease,” in *3D Printing Applications in Cardiovascular Medicine*. Elsevier, 2018, pp. 243–253.